

# Physics of Automated-Driving Vehicular Traffic

Boris S. Kerner<sup>1</sup>

<sup>1</sup> *Physics of Transport and Traffic, University of Duisburg-Essen, 47048 Duisburg, Germany*

We have found that a variety of phase transitions occurring between three traffic phases (free flow (F), synchronized flow (S), and wide moving jam (J)) determine the spatiotemporal dynamics of traffic consisting of 100% automated-driving vehicles moving on a two-lane road with an on-ramp bottleneck. This means that three-phase traffic theory is a common framework for the description of traffic states independent of whether human-driving or automated-driving vehicles move in vehicular traffic. To prove this, we have studied automated-driving vehicular traffic with the use of classical Helly's model (1959) widely applied for automated vehicle motion. Although dynamic rules of the motion of automated-driving vehicles in a road lane are qualitatively different from those of human-driving vehicles, we have revealed that a free-flow-to-synchronized-flow transition (F→S transition) exhibits the nucleation nature, which was observed in empirical field data measured in traffic consisting of 100% human-driving vehicles. The physics of the nucleation nature of the F→S transition in automated-driving traffic is associated with a discontinuity in the rate of lane-changing that causes the discontinuity in the rate of over-acceleration. This discontinuous character of over-acceleration leads to both the existence and self-maintaining of synchronized flow at the bottleneck in automated-driving vehicular traffic as well as to the existence at any time instant of a range of highway capacities between some minimum and maximum capacities. Within the capacity range, an F→S transition can be induced; however, when the maximum capacity is exceeded, then after some time-delay a spontaneous F→S transition occurs at the bottleneck. The phases F, S, and J can coexist each other in space and time.

PACS numbers: 89.40.-a, 47.54.-r, 64.60.Cn, 05.65.+b

## I. INTRODUCTION

In traffic of human-driving vehicles, traffic breakdown that is a transition from free flow to congested traffic occurs mostly at bottlenecks. Already in 1950s–1960s two classes of models for traffic breakdown were introduced:

(i) In the classical Lighthill-Whitham-Richards (LWR) model [1, 2], it is assumed that there is a fundamental diagram for traffic flow at a highway bottleneck; the maximum flow rate at the fundamental diagram is equal to highway capacity: If the flow rate upstream of a bottleneck exceeds the capacity, traffic breakdown occurs; otherwise, no traffic breakdown can occur at the bottleneck (see, e.g., [3–7]).

(ii) In 1958, Herman, Gazis, Montroll, Potts, Rothery and Chandler from General Motors (GM) Company [8–11] as well as by Kometani and Sasaki [12–15] assumed that traffic breakdown occurs due to traffic flow instability in vehicular traffic. This classical traffic instability was incorporated into a number of traffic flow models (e.g., papers, reviews, and books [6, 7, 16–33]). As found in [34], the classic traffic instability leads to a phase transition from free flow (F) to a wide moving jam (J) called an F→J transition.

It is commonly assumed that in future vehicular traffic automated-driving vehicles [automated vehicle (AV)] will play a decisive role (see, e.g., [35–49]). Automated-driving is realized through the use of an automated system in a vehicle that controls over the vehicle in traffic flow as well as through the use of cooperative driving realized through vehicle-to-vehicle

communication or/and through vehicle-to-infrastructure communication (see, e.g., [50–54]). In most studies of the effect of automated vehicles on mixed traffic consisting of random distribution of automated-driving and human-driving vehicles (e.g., see [55–89]), motion of human-driving vehicles is described with the use of the above-mentioned standard traffic flow models [1–33].

However, from a study of empirical field traffic data it was found that real traffic breakdown is a transition from free flow (F) to synchronized flow (S) called an F→S transition that occurs in metastable free flow with respect to an F→S transition at a bottleneck [90–92] (see for a review [93–97]): The F→S transition (traffic breakdown) exhibits the empirical nucleation nature (Fig. 1). The LWR theory [1–7] cannot explain the nucleation nature of real traffic breakdown. The classical traffic instability [6–34] that leads to the F→J transition [21–24, 27, 34] cannot also explain real traffic breakdown at highway bottlenecks [130].

To explain the empirical nucleation nature of traffic breakdown (F→S transition), the author introduced three-phase traffic theory [90–97]). The three-phase traffic theory is a framework for the description of empirical traffic data in three phases: Free flow (F), synchronized flow (S) and wide moving jam (J); the traffic phases S and J belong to congested traffic. The first implementations of the three-phase traffic theory in mathematical traffic flow models have been made in [100, 101]. These stochastic models have been further developed for different applications (see, e.g., [102]). Over time, other traffic flow models, which incorporate hypotheses of the three-phases traffic theory, have also been developed (see, e.g., [103–124]). With the use of a

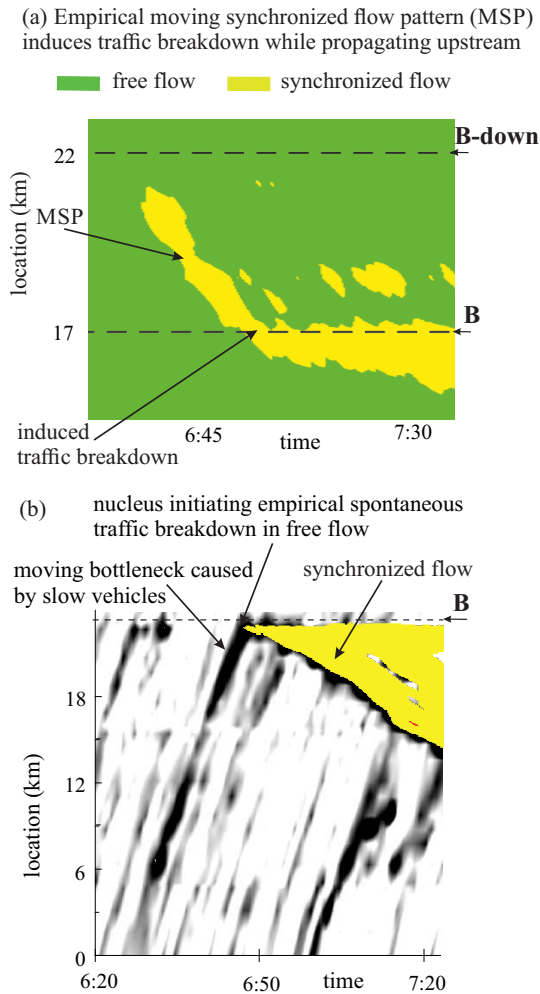


FIG. 1: Empirical nucleation nature of traffic breakdown (F→S transition) at bottlenecks in human-driving vehicular traffic; traffic data were measured with road detectors installed along road sections [90, 91, 93, 98]: (a) Speed data in space and time presented with averaging method of [99]: A moving synchronized flow pattern (MSP) that has emerged at downstream bottleneck (B-down) while propagating upstream induces F→S transition (induced traffic breakdown) at upstream on-ramp bottleneck (B). (b) One of the empirical waves (black colored waves) of decrease in the average speed caused by slow moving vehicles (moving bottleneck) while propagating downstream in free flow acts as a nucleus for spontaneous F→S transition (spontaneous traffic breakdown) at bottleneck (B) when the speed wave propagates through bottleneck B1. Adapted from [96].

microscopic three-phase traffic model for human-driving vehicles, the effect of a small share of automated vehicles on traffic breakdown in mixed traffic at bottlenecks has been studied in [125].

A basic hypothesis of the three-phase traffic theory is that in some traffic situations vehicle acceleration called *over-acceleration* exhibits a *discontinuous character* (Fig. 2): In synchronized flow, the probability of

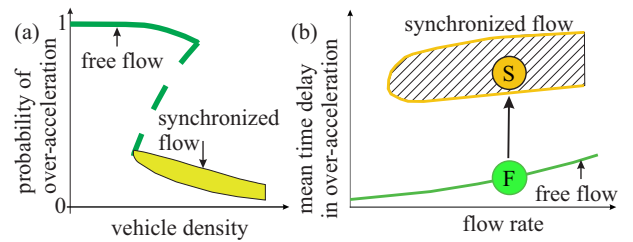


FIG. 2: Discontinuous character of over-acceleration [90, 91, 93]: (a) Qualitative presentation of over-acceleration probability during a given time interval. Equivalent presentation of (a) as a discontinuous dependence of the mean time delay in over-acceleration on the flow rate; F and S are states of free flow and synchronized flow, respectively. Adapted from [93, 96].

over-acceleration is considerably lower than it is in free flow [90, 91, 93] [131]. It has been shown that the discontinuous character of over-acceleration causes a metastability of free flow with respect to the F→S transition; in its turn, this metastability explains the empirical nucleation nature of traffic breakdown observed in measured field traffic data. The three-phase traffic theory has been initially created for the description of empirical *human-driving* vehicular traffic [90–96].

The objective of this paper is to show that the spatiotemporal dynamics of traffic consisting of 100% automated-driving vehicles is described in the framework of three-phase traffic theory. It should be emphasized that dynamic rules of motion of automated vehicles in a road lane can be developed that are totally different from the real dynamic behavior of human-driving vehicles. Therefore, a question can arise:

- Why should the three-phase traffic theory describe spatiotemporal phase transitions in traffic flow consisting of 100% of automated vehicles whose dynamics rules of motion in road lane can be totally different from the real dynamic behavior of human-driving vehicles?

To answer this question, we should recall that one of the mechanisms of over-acceleration exhibiting the discontinuous character (Fig. 2) is vehicle acceleration through lane-changing to a faster lane on a multi-lane road [90, 91, 93] [132]. Either a human-driving or automated-driving vehicle changes to a neighborhood target lane if (i) some *incentive conditions* for lane changing (like the vehicle can pass the preceding vehicle or/and move faster in the target lane) *and* (ii) some *safety conditions* for lane-changing are satisfied, at which no collisions between vehicles can occur. Thus, if the discontinuous character of over-acceleration due to lane-changing to a faster lane (Fig. 2) is realized for human-driving vehicles, it should be also for automated vehicles: The discontinuous character of over-acceleration can be assumed to be an universal

physical feature of vehicular traffic.

The paper is organized as follows: In Sec. II, we consider a microscopic model of automated-driving vehicular traffic on a two-lane road and study the physics of the nucleation nature of the F→S transition at a bottleneck. The existence of a range of highway capacities at any time instant is the subject of Sec. III. In Sec. IV, a generalization of nucleation features of the F→S transition in automated-driving traffic is made. Transitions between the three phases F, S, and J in automated-driving traffic are studied in Sec. V. In discussion (Sec. VI), we show that the basic result about the nucleation nature of the F→S transition at the bottleneck remains for string-unstable automated-driving traffic and even if a different model for automated-driving vehicles is used.

## II. PHYSICS OF METASTABILITY OF AUTOMATED-DRIVING VEHICULAR TRAFFIC AT BOTTLENECK WITH RESPECT TO F→S TRANSITION

### A. Model of automated-driving vehicular traffic on two-lane road with on-ramp bottleneck

We study a model of vehicular traffic consisting of 100% identical automated vehicles moving on a two-lane road with an on-ramp bottleneck. We assume that the control over an automated vehicle moving in a road lane is realized through an adaptive cruise control system (ACC) that is described by a classical model in which the acceleration (deceleration)  $a$  of the automated vehicle is determined by the space gap to the preceding vehicle  $g = x_\ell - x - d$  and the relative speed  $\Delta v = v_\ell - v$  measured by the automated vehicle as well as by some optimal space gap  $g_{\text{opt}}$  between the automated vehicle and the preceding automated vehicle (see, e.g., [36–40, 46–48]):

$$a = K_1(g - g_{\text{opt}}) + K_2\Delta v, \quad (1)$$

where  $x$  and  $v$  are the coordinate and the speed of the automated vehicle,  $x_\ell$  and  $v_\ell$  are the coordinate and the speed of the preceding automated vehicle,  $d$  is the vehicle length; here and below  $v$ ,  $v_\ell$ , and  $g$  are time-functions;  $K_1$  and  $K_2$  are constant coefficients of vehicle adaptation;

$$g_{\text{opt}} = v\tau_d, \quad (2)$$

$\tau_d$  is a desired time headway of the automated vehicle to the preceding automated vehicle. The classical model (1), (2) that is currently used in most studied of automated-driving in a road lane [36–40, 46–48] is related to Helly's car-following model [126]. The motion of the automated vehicle in a road lane is found under conditions  $0 \leq v \leq v_{\text{free}}$  from the solution of equations  $dv/dt = a$ ,  $dx/dt = v$  [133], where the maximum speed (in free flow)  $v_{\text{free}}$  is a constant. There can be string instability of a long enough platoon of automated vehicles

(1), (2) [36–40, 46–48]. As found by Liang and Peng [38], coefficients  $K_2$  and  $K_1$  in (1) can be chosen to satisfy condition for string stability

$$K_2 > (2 - K_1\tau_d^2)/2\tau_d. \quad (3)$$

In the main text of the paper (Secs. II–V), we consider only automated vehicles whose parameters satisfy condition (3) for string stability[134].

We use incentive lane changing rules from the right to left lane R→L (4) and from the left to right lane L→R (5) as well as safety conditions (6) known for human-driving vehicles (see, e.g., [127])

$$R \rightarrow L : v^+(t) \geq v_\ell(t) + \delta_1 \text{ and } v(t) \geq v_\ell(t), \quad (4)$$

$$L \rightarrow R : v^+(t) \geq v_\ell(t) + \delta_2 \text{ or } v^+(t) \geq v(t) + \delta_2, \quad (5)$$

$$g^+(t) \geq v(t)\tau_2, \quad g^-(t) \geq v^-(t)\tau_1, \quad (6)$$

at which the automated vehicle changes to the faster target lane with the objective to pass a slower automated vehicle in the current lane if time headway to preceding and following vehicles in the target lane are not shorter than some given safety time headway  $\tau_1$  and  $\tau_2$ . In (4)–(6), superscripts + and – denote, respectively, the preceding and the following vehicles in the target lane;  $\tau_1$ ,  $\tau_2$ ,  $\delta_1$ ,  $\delta_2$  are positive constants.

Open boundary conditions are applied. At the beginning of the two-lane road  $x = 0$  vehicles are generated one after another in each of the lanes of the road at time instants  $t^{(k)} = k\tau_{\text{in}}$ ,  $k = 1, 2, \dots$ , where  $\tau_{\text{in}} = 1/q_{\text{in}}$ ,  $q_{\text{in}}$  is a given time-independent flow rate per road lane. The initial vehicle speed is equal to  $v_{\text{free}}$ . After a vehicle has reached the end of the road  $x = L$  it is removed. Before this occurs, the farthest downstream vehicle maintains its speed and lane.

In the on-ramp model, there is a merging region of length  $L_m$  in the right road lane that begins at road location  $x = x_{\text{on}}$  within which automated vehicles can merge from the on-ramp. Vehicles are generated at the on-ramp one after another at time instants  $t^{(m)} = m\tau_{\text{on}}$ ,  $m = 1, 2, \dots$ , where  $\tau_{\text{on}} = 1/q_{\text{on}}$ ,  $q_{\text{on}}$  is the on-ramp inflow rate. To reduce a local speed decrease occurring through the vehicle merging at the on-ramp bottleneck, as assumed for many known cooperative automated driving scenarios, automated vehicles merge with the speed of the preceding vehicle  $v^+$  at a middle location  $x = (x^+ + x^-)/2$  between the preceding and following vehicles in the right lane, when the space gap between the vehicles exceeds some safety value  $g_{\text{target}}^{(\text{min})} = \lambda_b v^+ + d$ , i.e., some safety condition  $x^+ - x^- - d > g_{\text{target}}^{(\text{min})}$  should be satisfied. In accordance with these merging conditions, the space gap for a vehicle merging between each pair of consecutive vehicles in the right road lane is checked, starting from the upstream boundary of the merging region. If there is such a pair of consecutive vehicles, the vehicle merges onto the right road lane; if there is no pair of consecutive vehicles, for which the safety condition is satisfied at the current time step, the procedure is repeated at the next time step, and so on.

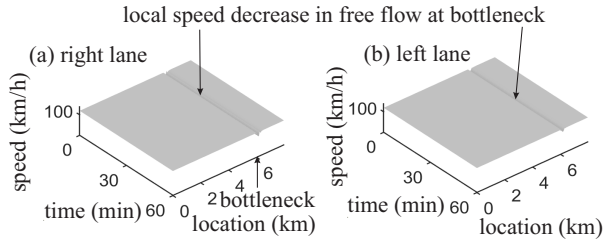


FIG. 3: Simulations with model of Sec.II A of the occurrence of local speed decrease in free flow on two-lane road at bottleneck: Speed in space and time in the right lane (a) and the left lane (b).  $q_{in} = 2571$  (vehicles/h)/lane,  $q_{on} = 720$  vehicles/h. Parameters of automated vehicles:  $\tau_d = 1$  s,  $K_1 = 0.3$  s<sup>-2</sup>,  $K_2 = 0.9$  s<sup>-1</sup>,  $v_{free} = 120$  km/h,  $d = 7.5$  m. Lane-changing parameters:  $\delta_1 = 1$  m/s,  $\delta_2 = 5$  m/s,  $\tau_1 = 0.6$  s,  $\tau_2 = 0.2$  s. Road and on-ramp parameters: road length  $L = 8$  km,  $x_{on} = 6$  km,  $L_m = 0.3$  km,  $\lambda_b = 0.3$  s.

When free flow is realized at the bottleneck, we have found a known result that due to R→L lane-changing the on-ramp inflow is distributed between two lanes that causes the occurrence of local speed decreases in both the right and left road lanes at the bottleneck (Fig. 3).

### B. Free flow metastability at bottleneck

As mentioned, rules of vehicle motion of Sec. II A as well as the occurrence of local speed decreases in both road lanes at the bottleneck in free flow are known in vehicular traffic theory. Nevertheless, we have revealed that the free flow state at the bottleneck shown in Fig. 3 is in a metastable state with respect to an F→S transition.

To prove this result, at a time instant  $T_{ind}$  we have disturbed the free flow state at the bottleneck shown in Fig. 3 through the application of a time-limited on-ramp inflow impulse  $\Delta q_{on}$  of some duration  $\Delta t$  (Fig. 4): (i) At time interval  $0 \leq t < T_{ind}$ , the on-ramp inflow rate  $q_{on}$  is the same as that in Fig. 3 and, therefore, the same free flow state is realized; (ii) during the impulse  $T_{ind} \leq t \leq T_{ind} + \Delta t$  the on-ramp inflow rate has increased to a large enough value  $q_{on} + \Delta q_{on}$  at which traffic congestion is realized at the bottleneck; (iii) at time  $t > T_{ind} + \Delta t$ , although the on-ramp inflow rate has reduced to its initial value  $q_{on}$ , rather the free flow state returns at the bottleneck, congested traffic persists at the bottleneck. The downstream front of induced congested traffic is fixed at the bottleneck while the upstream front of congested traffic is continuously propagate upstream (Fig. 4). In accordance with the phase definitions made in three-phase traffic theory [93], the induced congested traffic belongs to the synchronized flow phase of automated-driving vehicular traffic. Thus, at the same on-ramp inflow rate  $q_{on}$  there can be either a free flow state or a synchronized flow state at the bottleneck, i.e., free flow in Fig. 3 is indeed in a metastable state with

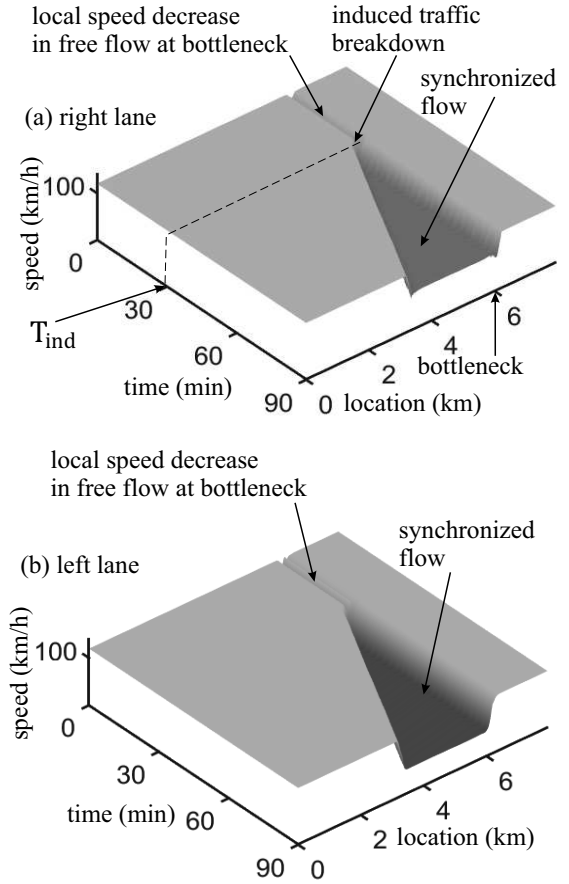


FIG. 4: Proof of the metastability of free flow state shown in Fig. 3 in automated-driving vehicular traffic moving on two-lane road with bottleneck: Speed in space and time in the right lane (a) and left lane (b). Parameters of on-ramp inflow-rate impulse inducing F→S transition at bottleneck:  $T_{ind} = 30$  min,  $\Delta q_{on} = 180$  vehicles/h,  $\Delta t = 2$  min. Other model parameters are the same as those in Fig. 3.

respect to an F→S transition at the bottleneck.

### C. Discontinuity in the rate of over-acceleration through lane-changing

To explain the physics of the free flow metastability with respect to the F→S transition (Sec. IID), we should first explain here that there is a *discontinuity* in the rate of R→L lane-changing denoted by  $R_{RL}$  [135]. The discontinuity in the rate of R→L lane-changing is realized due to the F→S transition, i.e., when free flow transforms into synchronized flow. Examples of R→L lane-changing in free flow and synchronized flow are shown, respectively, in Figs. 5 and 6 through the use of dashed vertical lines R→L. In free flow occurring during time  $0 \leq t < T_{ind}$ , we have found  $R_{RL} \approx 6.1$  min<sup>-1</sup>, whereas in synchronized flow that occurs at the bottleneck at  $t > T_{ind} + \Delta t$ , we have found that R→L

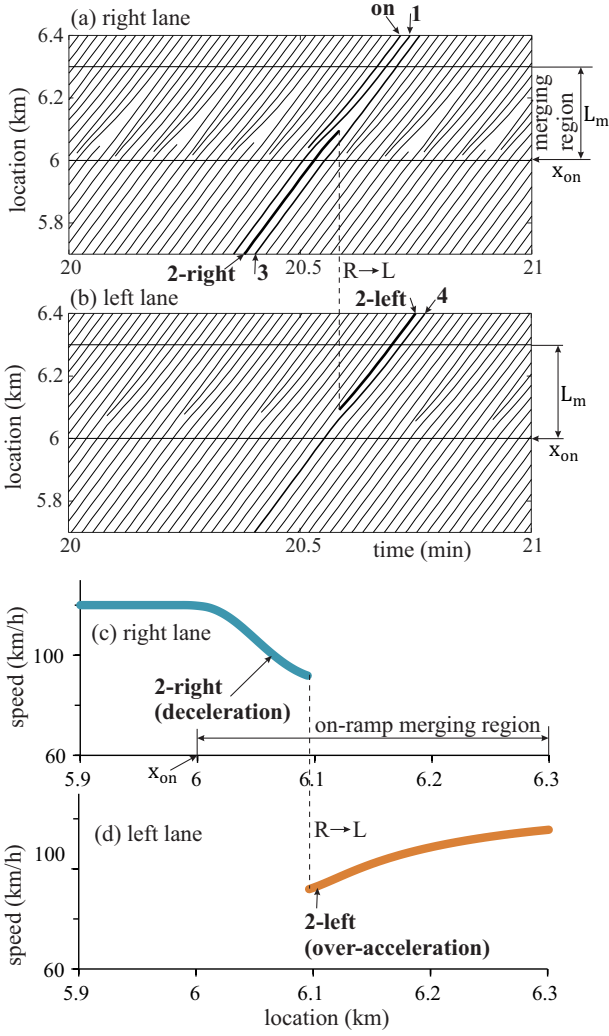


FIG. 5: Continuation of Figs. 3 and 4. (a, b) Simulated vehicle trajectories within local speed decrease in free flow at bottleneck in the right lane (a) and left lane (b) at time  $t < T_{\text{ind}} + \Delta t$ . (c, d) Location-functions of speed of vehicle 2 labeled by “2-right” in the right lane (c) and by “2-left” in left lane (d) in (a, b). R→L lane-changing of vehicle 2 is marked by dashed vertical lines R→L.

lane-changing rate  $R_{\text{RL}}$  reduces sharply to  $R_{\text{RL}} \approx 2.8 \text{ min}^{-1}$ . To explain the abrupt reduction of the rate of R→L lane-changing  $R_{\text{RL}}$  occurring due to the F→S transition, we mention that in synchronized flow, the mean time headway between vehicles  $\tau_{\text{mean}}^{(\text{syn})}$  reduces while becoming close to  $\tau_d = 1 \text{ s}$ . At this short time headway, safety conditions for lane changing (6) is more difficult to satisfy in comparison with free flow for which  $\tau_{\text{mean}}^{(\text{free})} \approx 1.175 \text{ s}$  [136]. The difference in values of  $R_{\text{RL}}$  in free flow and synchronized flow can already be seen from a comparison of two fragments of vehicle trajectories in the vicinity of the on-ramp merging region shown for free flow in Fig. 5 [137] and for synchronized flow in Fig. 6.

R→L lane-changing of a vehicle that has initially

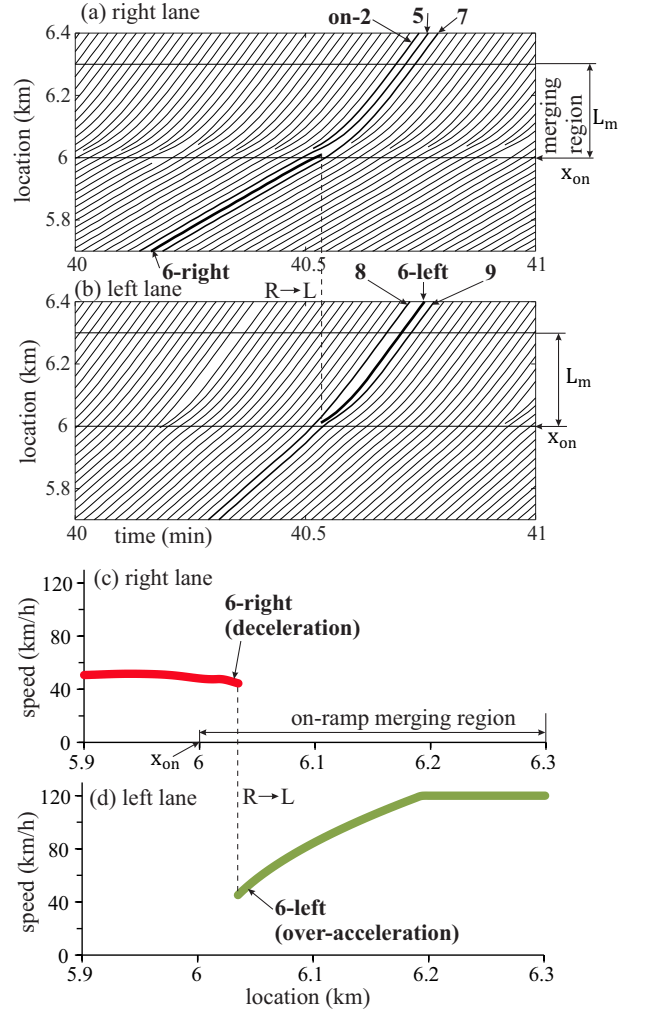


FIG. 6: Continuation of Fig. 4. (a, b) Simulated vehicle trajectories in synchronized flow at bottleneck in the right lane (a) and left lane (b) at time  $t > T_{\text{ind}} + \Delta t$ . (c, d) Location-functions of speed of vehicle 6 labeled by “6-right” in the right lane (c) and by “6-left” in left lane (d) in (a, b). R→L lane-changing of vehicle 6 is marked by dashed vertical lines R→L.

decelerated in the right lane (for example, vehicle 2-right in Figs. 5 (a, c) and vehicle 6-right in Figs. 6 (a, c) have decelerated before R→L lane-changing) leads to the acceleration of the vehicle in the left lane. Indeed, in free flow, vehicle 2-left in Figs. 5 (b, d) accelerates after R→L lane-changing. In synchronized flow, vehicle 6-left in Figs. 6 (b, d) also accelerates after R→L lane-changing. The vehicle acceleration under consideration is solely determined by R→L lane-changing of the vehicle. Thus, the rate of the vehicle acceleration denoted by  $R_{\text{OA}}$ , which is caused by R→L lane-changing, is given by formula

$$R_{\text{OA}} = R_{\text{RL}}. \quad (7)$$

Thus, vehicle acceleration caused by R→L lane-changing

exhibits the discontinuous character: In accordance with (7), there is the discontinuity in the rate of vehicle acceleration  $R_{OA}$  when free flow transforms into synchronized flow.

In next Sec. IID, we explain that the discontinuity in the rate of vehicle acceleration  $R_{OA}$  caused by R→L lane-changing leads to the free flow metastability with respect to the F→S transition (Fig. 4); in three-phase traffic theory, such vehicle acceleration has been called *over-acceleration* [93, 96]. Therefore, the acceleration of vehicle 2-left in free flow in Figs. 5 (b, d) as well as the acceleration of vehicle 6-left in synchronized flow (Figs. 6 (b, d)) are examples of over-acceleration; this explains the use of the term *over-acceleration* in Figs. 5 and 6. We consider also the mean time delay in over-acceleration denoted by  $T_{OA}$  that is equal to  $1/R_{OA}$ ; in free flow  $T_{OA} \approx 9.84$  s, whereas in synchronized flow  $T_{OA} \approx 21.4$  s. The discontinuities in the rate  $R_{OA}$  and mean time delay  $T_{OA}$  of over-acceleration, i.e., the discontinuous character of over-acceleration found here for automated-driving vehicular traffic is in agreement with three-phase traffic theory for human-driving traffic (Fig. 2).

#### D. Spatiotemporal competition of speed adaptation with over-acceleration

There is a spatiotemporal competition between over-acceleration and speed adaptation. In this competition, there are a tendency to free flow and the opposite tendency to synchronized flow. The tendency to free flow is through over-acceleration. The opposite tendency to synchronized flow is through speed adaptation.

Speed adaptation is vehicle deceleration occurring when a vehicle approaches a slower moving preceding vehicle and the following vehicle cannot pass it. We should distinguish speed adaptation in the right lane and speed adaptation in the left lane. This is because speed adaptation in the left lane is caused by a dual role of R→L lane-changing.

##### 1. Tendency to free flow through over-acceleration

In free flow (Fig. 5) and synchronized flow (Fig. 6), over-acceleration through vehicle lane-changing to the left lane permits the following vehicle remaining in the right lane to accelerate. When free flow is currently at the bottleneck, the tendency to free flow is through over-acceleration that maintains the free flow state. Indeed, due to over-acceleration of vehicle 2 through its changing to the left lane (“2-left (over-acceleration)” in Fig. 7 (a)), the following vehicle 3 remaining in the right lane that trajectory is shown in Fig. 5 (a) accelerates (labeled by “3, acceleration” in Fig. 7 (a)). When synchronized flow is currently at the bottleneck, the tendency caused by over-acceleration tries to transform

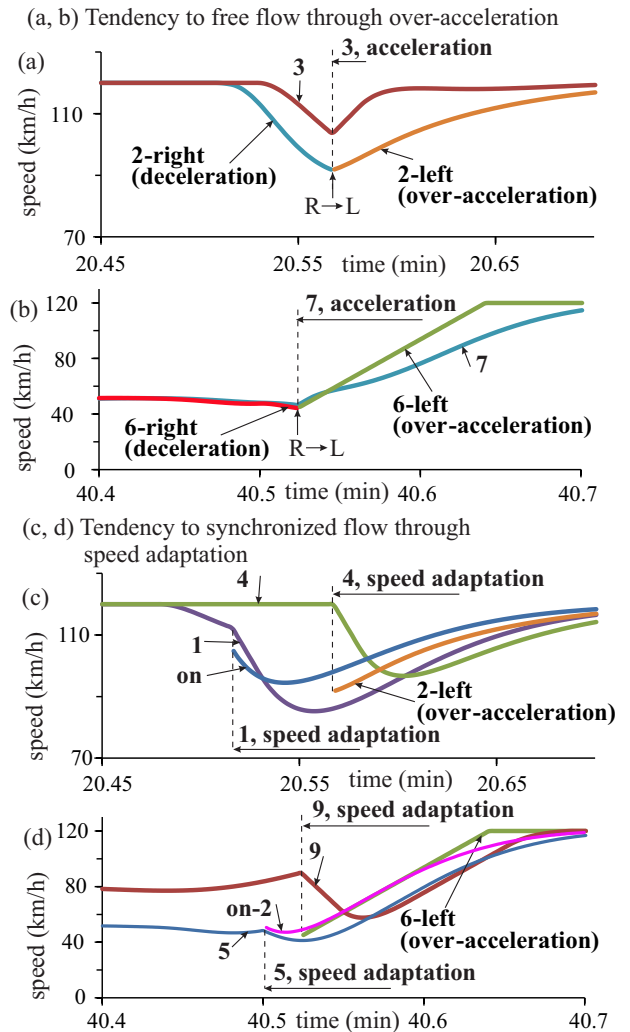


FIG. 7: Simulations of spatiotemporal competition between over-acceleration and speed adaptation. Time-functions of speed for vehicle trajectories presented in Figs. 5 (a, b) and 6 (a, b) labeled by the same numbers, respectively: (a, b) Tendency to free flow. (c, d) Tendency to synchronized flow.

synchronized flow to a free flow state. For example, due to over-acceleration of vehicle 6 through its changing to the left lane (“6-left (over-acceleration)” in Fig. 7 (b)) the following vehicle 7 remaining in the right lane that trajectory is shown in Fig. 6 (a) accelerates (labeled by “7, acceleration” in Fig. 7 (b)).

##### 2. Tendency to synchronized flow through speed adaptation in the right lane

When free flow is at the bottleneck, the tendency caused by speed adaptation tries to transform free flow to a synchronized flow (Fig. 7 (c)). A vehicle merging from the on-ramp (vehicle “on” in Figs. 5 (a) and 7 (c)), forces the following vehicle 1 that trajectory is shown in Fig. 5

(a) to decelerate (“1, speed adaptation” in Fig. 7 (c)) while adapting the speed to the slower merging vehicle “on”.

If synchronized flow is at the bottleneck, the tendency caused by speed adaptation tries to maintain the synchronized flow state (Fig. 7 (d)). A vehicle merging from the on-ramp (vehicle “on-2” in Figs. 6 (a) and 7 (d)), forces the following vehicle 5 that trajectory is shown in Fig. 6 (a) to decelerate (labeled by “5, speed adaptation” in Fig. 7 (d)).

### 3. Tendency to synchronized flow through speed adaptation in the left lane: Dual role of lane-changing

There is a dual role of lane-changing that is as follows. In free flow, lane-changing of vehicle 2 leads to over-acceleration (“2-left (over-acceleration)” in Figs. 5 (a, d)). Contrarily, the same lane-changing of vehicle 2 causes speed adaptation in the left lane. Indeed, the following vehicle 4 in the left lane that trajectory is shown in Fig. 6 (b) must decelerate (“4, speed adaptation” in Fig. 7 (d)), while adapting its speed to the speed of slower vehicle 2 that has just changed from the right lane to left lane.

Speed adaptation caused by a dual role of lane-changing occurs also in synchronized flow. An example is lane-changing of vehicle 6 (“6-left (over-acceleration)” in Fig. 7 (d)) that forces the following vehicle 9 in the left lane that trajectory is shown in Fig. 6 (b) to decelerate (“9, speed adaptation” in Fig. 7 (d)).

### 4. Two possible results of competition between over-acceleration and speed adaptation

In Fig. 5, free flow persists at the bottleneck. This means that at the over-acceleration rate  $R_{OA} \approx 6.1 \text{ min}^{-1}$  the tendency to free flow through over-acceleration overcomes the tendency to synchronized flow through speed adaptation. The result of the competition between over-acceleration and speed adaptation is the occurrence of the local speed decrease at the bottleneck without the emergence of synchronized flow (Figs. 3 and 4).

Contrarily, in Fig. 6 synchronized flow persists at the bottleneck (labeled by “synchronized flow”). This means that the tendency to synchronized flow through speed adaptation overcomes the tendency to free flow through over-acceleration. This is because the over-acceleration rate  $R_{OA} \approx 2.8 \text{ min}^{-1}$  becomes too small in synchronized flow. The competition between speed adaptation and over-acceleration determines the speed in synchronized flow. However, due to the small rate of over-acceleration in synchronized flow this competition cannot cause a return transition from synchronized flow to free flow.

Thus, the cause of the free flow metastability with respect to the F→S transition (Fig. 4) is a spatiotemporal

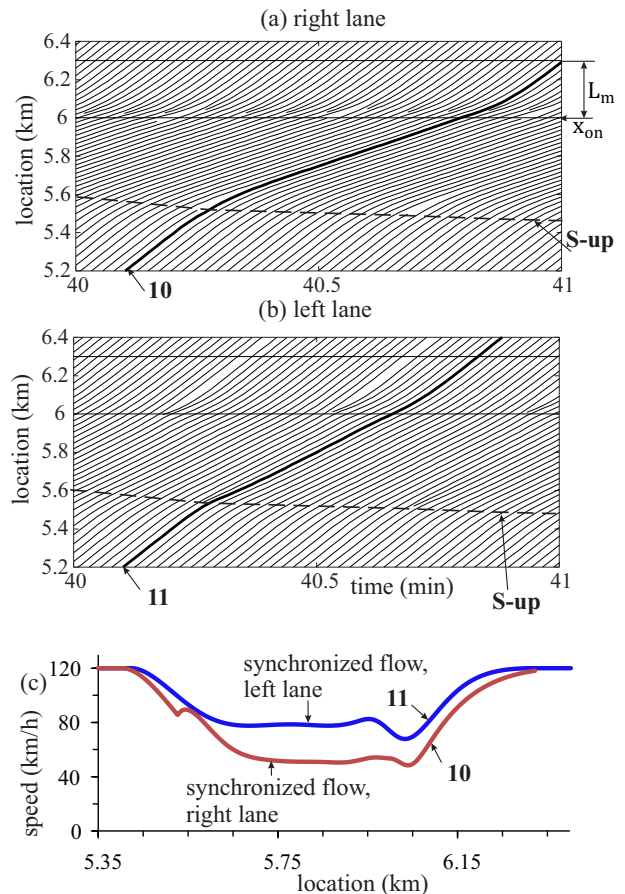


FIG. 8: Continuation of Fig. 6. Features of synchronized flow: (a, b) Vehicle trajectories at  $t > T_{ind} + \Delta t$ , i.e., after F→S transition has occurred at the bottleneck. (c, d) Location-functions of speeds for vehicles 10 and 11 in (a, b).

competition between over-acceleration, which exhibits the discontinuous character, and speed adaptation.

## E. Synchronized flow characteristics

### 1. Synchronization of velocities of upstream fronts of synchronized flow in road lanes

The speed in synchronized flow in the right lane (vehicle 10 in Fig. 8) is less than the speed in synchronized flow in the left lane (vehicle 11). However, this speed difference does not lead to different velocities of the upstream fronts of synchronized flow in the left and right lanes: These upstream front velocities are synchronized (upstream fronts of synchronized flow are labeled by dashed curves “S-up” in Fig. 8 (a, b)).

The physics of this synchronization effect is associated with R→L lane-changing that occurs in the vicinity of the upstream synchronized flow front in the right lane (Fig. 9). While approaching the upstream front of

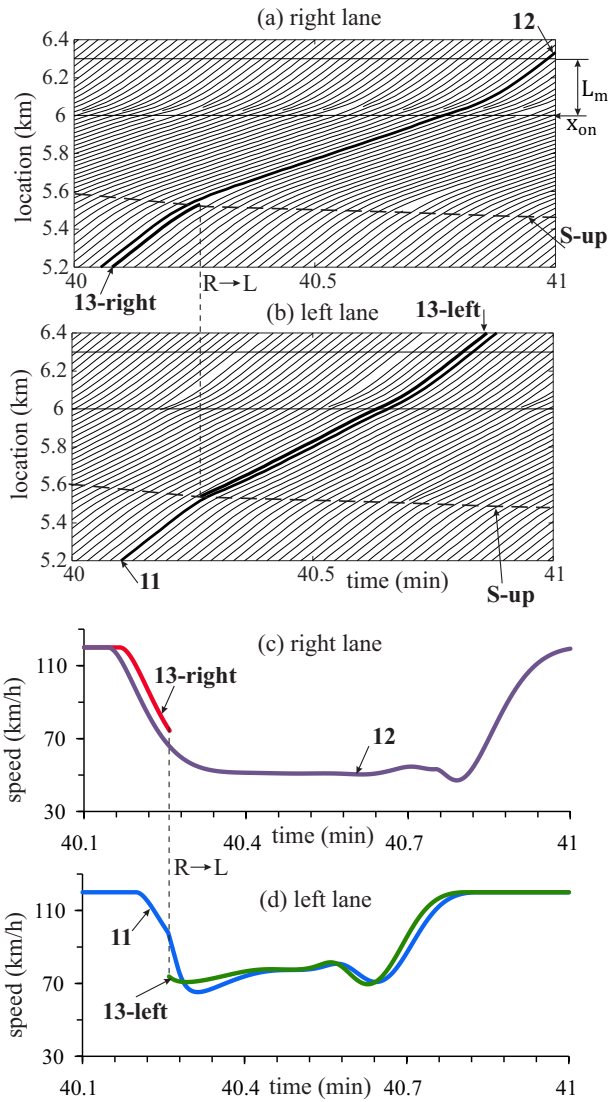


FIG. 9: Continuation of Fig. 8: Synchronization of velocities of upstream fronts of synchronized flow in the right and left lanes. (a, b) Vehicle trajectories taken from Fig. 8 (a, b). (c, d) Time-functions of speeds along trajectories marked in (a, b) by the same numbers, respectively.

synchronized flow in the right lane, vehicles decelerate (e.g., vehicle 12 in Fig. 9 (a, c)). When the upstream front of synchronized flow in the left lane comes even slightly downstream of the upstream front of synchronized flow in the right lane, free flow is realized in the left lane between these upstream synchronized flow fronts; then, between the fronts lane-changing rate  $R_{RL}$  increases. This causes R→L lane-changing of a vehicle decelerating to a synchronized flow speed in the vicinity of the upstream front of synchronized flow in the right lane (example of R→L lane-changing for vehicle 13 is marked by dashed vertical lines labeled by R→L in Fig. 9). Due to the lane-changing of a slow moving vehicle 13-right to the left lane (vehicle 13-left), the

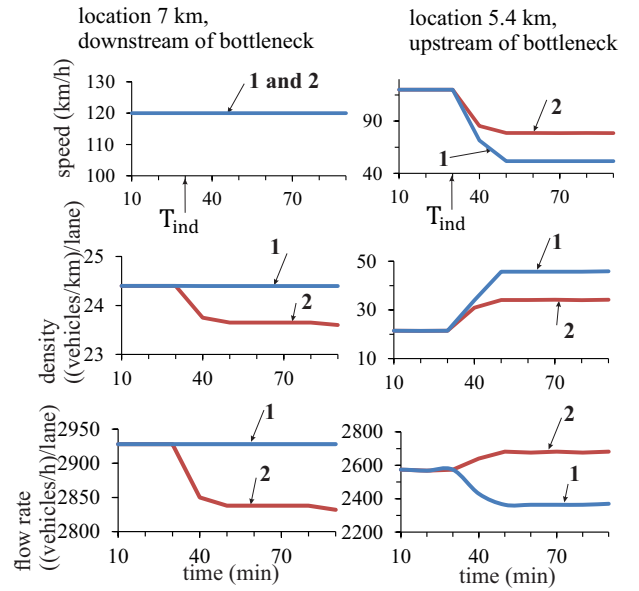


FIG. 10: Continuation of Fig. 4: Time-functions of automated vehicle speed (first line), density (second line), and flow rate (third line) at road location  $x = 7$  km [downstream of the bottleneck] (left column) and road location  $x = 5.4$  km [upstream of the bottleneck] (right column); curves 1 – right lane, curves 2 – left lane. 10 min averaging time interval at virtual detectors.

following vehicle 11 in the left lane begins to decelerate stronger than it has been before lane-changing (Fig. 9 (d)). This leads to the synchronization of the upstream front velocities.

## 2. Effect of discontinuity in lane-changing rate on flow-rate distribution

In the initial free flow state existing at the bottleneck at  $0 \leq t < T_{ind}$  (Fig. 4), R→L lane-changing leads to the nearly fully equalization of the flow rates and densities between the road lanes downstream of the bottleneck (left column in Fig. 10 at  $t < T_{ind} = 30$  min). After the F→S transition has occurred, the lane-changing rate in synchronized flow at the bottleneck decreases sharply (discontinuity in the lane-changing rate) and, therefore, the flow rates and densities between lanes cannot be equalized. This explains why in free flow downstream of the bottleneck both the density and flow rate are smaller in the left lane than they are, respectively, in the right lane (left column in Fig. 10 at  $t \geq T_{ind}$ ).

The discontinuity in the lane-changing rate is also responsible for differences in the averaged speeds, densities, and flow rates in synchronized flow in the right and left lanes upstream of the bottleneck (right column in Fig. 10 at  $t \geq T_{ind}$ ).



### F. Three-phase traffic theory as common framework for human-driving and automated-driving traffic

Simulations of automated-driving vehicular traffic (Figs. 11 (a, b)) show the empirical nucleation features of the F→S transition found in measurements of real human-driving traffic (Figs. 1 (a, b)). Thus, three-phase traffic theory can indeed be considered a common framework for the analysis of the dynamics of human-driving and automated-driving traffic.

A moving synchronized flow pattern (MSP) in Fig. 11 (a) has been induced through the use of an on-ramp inflow impulse at a downstream bottleneck (B-down in Fig. 12). While propagating upstream, the MSP induces the F→S transition at the upstream bottleneck.

To simulate a moving bottleneck (MB) in Fig. 11 (b), we have assumed that there is a single automated vehicle moving in the right lane at a maximum free flow speed  $v_{MB}$  that is less than  $v_{free}$ . Already at  $v_{MB} = 110$  km/h that is only 10 km/h less than  $v_{free}$ , the slower vehicle acts as the MB (Figs. 11 (b) and 13). We have also assumed that through the use of cooperative-driving automated vehicles receive the information about the location and speed of the MB. Within a MB merging region of length  $L_M$ , each vehicle moving in the right lane changes to the left lane to pass the MB if safety conditions (6) are satisfied (e.g., see vehicle 1 in Figs. 13 (a, b)); lane-changing rules (4), (5) are not applied within the MB merging region [138]. Other vehicles for which conditions (6) are not satisfied have to move at the velocity  $v_{MB}$  behind the MB (trajectories of these vehicles are within a region between the MB trajectory and a dashed-dotted line in Fig. 13 (a)). Some vehicles moving in the left lane, after they have passed the MB location, change back to the right lane where they can move at the speed  $v_{free}$  (vehicle 2 in Figs. 13 (a, b)).

The MB causes a speed decrease localized at the MB that moves at the speed  $v_{MB}$  (Fig. 13 (c)). As in human-driving traffic (Fig. 1 (b)), when the local speed decrease at the MB reaches other local speed decrease at the on-ramp bottleneck, an additional short-time local speed decrease occurs at the bottleneck; this acts as a nucleus for traffic breakdown (F→S transition) at the bottleneck (Figs. 11 (b) and 13).

## III. RANGE OF HIGHWAY CAPACITIES AT ANY TIME INSTANT

### A. Minimum and maximum highway capacities

We have found that at any time instant the metastability of free flow in automated-driving vehicular traffic on two-lane road with the bottleneck is realized within a flow rate range

$$C_{min} \leq q_{sum} < C_{max}, \quad (8)$$

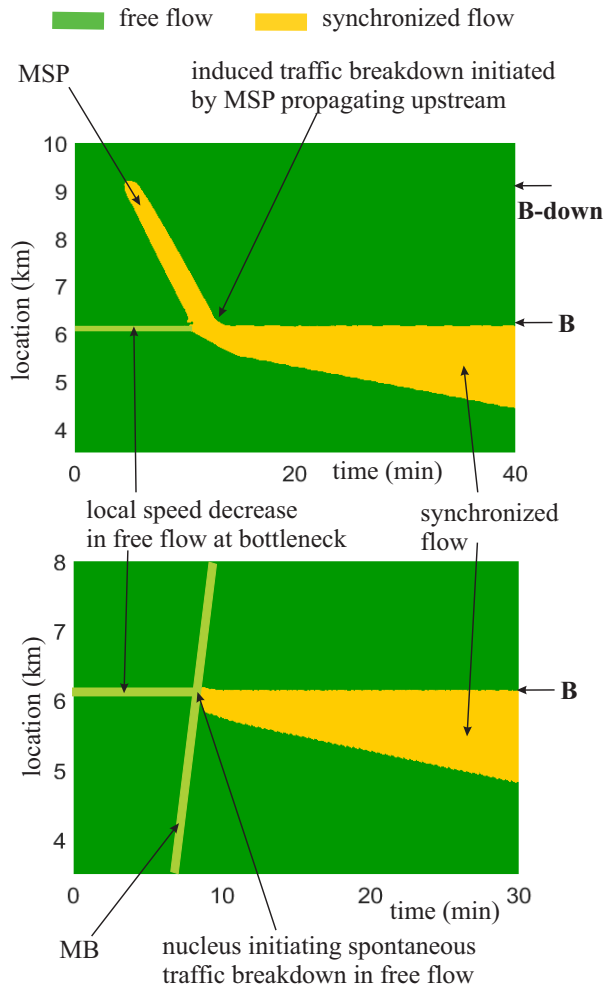


FIG. 11: Simulations of automated-driving vehicular traffic that reproduce empirical breakdown nucleation features measured in real human-driving traffic (Fig. 1). Speed data averaged across two-lane road are presented in space and time in free flow (green) and synchronized flow (yellow): (a) A moving synchronized flow pattern (MSP) induced at the downstream bottleneck (B-down) propagates upstream; reaching the upstream on-ramp bottleneck (B) the MSP induces the F→S transition at the bottleneck. (b) A slow moving vehicle (moving bottleneck – MB) while propagating downstream in free flow acts as a nucleus for empirical spontaneous F→S transition at bottleneck B when the MB propagates through bottleneck B. Both bottleneck B-down and bottleneck B are identical with the on-ramp bottleneck used above (Figs. 3–10); more details of simulations are in Figs. 12 and 13.

where  $q_{sum} = 2q_{in} + q_{on}$  is the total flow rate across the road in free flow;  $C_{min}$  and  $C_{max}$  are, respectively, minimum and maximum highway capacities. The physics of the capacity range (8) is that within this capacity range an F→S transition can be induced at the bottleneck. This result is in accordance with the three-phase traffic theory of human-driving traffic.

The minimum capacity  $C_{min}$  is explained in Fig. 14:

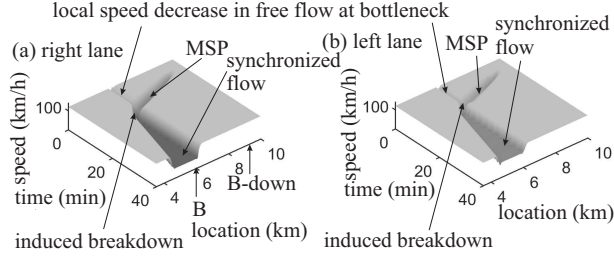


FIG. 12: Simulations of  $F \rightarrow S$  transition through upstream propagation of MSP to upstream bottleneck that in simplified version is shown in Fig. 11 (a): Speed in space and time in the right lane (a) and left lane (b).  $q_{in} = 2571$  (vehicles/h)/lane. Two-lane road with two bottlenecks: Parameters of upstream bottleneck (B) are  $x_{on} = 6$  km,  $L_m = 0.3$  km,  $q_{on} = 720$  vehicles/h; parameters of downstream bottleneck (B-down) are  $x_{on}^{(down)} = 9$  km,  $L_m^{(down)} = 0.3$  km,  $q_{on}^{(down)} = 0$ ; road length  $L = 10$  km. Parameters of on-ramp inflow impulse at downstream bottleneck B-down applied at  $T_{ind}^{(down)} = 5$  min are  $\Delta q_{on}^{(down)} = 900$  vehicles/h,  $\Delta t^{(down)} = 1$  min. Other model parameters are the same as those in Fig. 3.

At a given  $q_{in}$ , there is a minimum on-ramp inflow rate denoted by  $q_{on} = q_{on,min}$  at which in an initial free flow at the bottleneck (Fig. 14 (a)) an  $F \rightarrow S$  transition can still be induced (Fig. 14 (b)); the minimum capacity is equal to  $C_{min} = 2q_{in} + q_{on,min}$ . At the model parameters, the  $F \rightarrow S$  transition leads to the formation of a localized synchronized flow pattern (LSP) at the bottleneck (Fig. 14 (b)). Contrarily, if

$$q_{sum} < C_{min}, \quad (9)$$

no  $F \rightarrow S$  transition can be induced at the bottleneck: synchronized flow induced at the bottleneck dissolves over time (labeled by “dissolving synchronized flow” in Fig. 14 (c)).

When the flow rate  $q_{sum}$  increases, a maximum highway capacity  $C_{max}$  can be reached. The maximum capacity  $C_{max}$  is a total flow rate  $q_{sum}$  that separates two qualitatively different phenomena: (i) When condition (8) is satisfied, then free flow is in a metastable state with respect to the  $F \rightarrow S$  transition at the bottleneck (Figs. 4 and 14 (b)). (ii) When condition

$$q_{sum} > C_{max} \quad (10)$$

is satisfied, then free flow is in an unstable state with respect to a *spontaneous*  $F \rightarrow S$  transition at the bottleneck (Fig. 15). At a given flow rate  $q_{in}$ , the increase in  $q_{sum}$  is achieved through the increase in  $q_{on}$ . In this case, the maximum capacity  $C_{max}$  is reached, when the on-ramp inflow rate  $q_{on}$  is equal to some critical value denoted by  $q_{on} = q_{on,max}$ , i.e.,  $C_{max} = 2q_{in} + q_{on,max}$ .

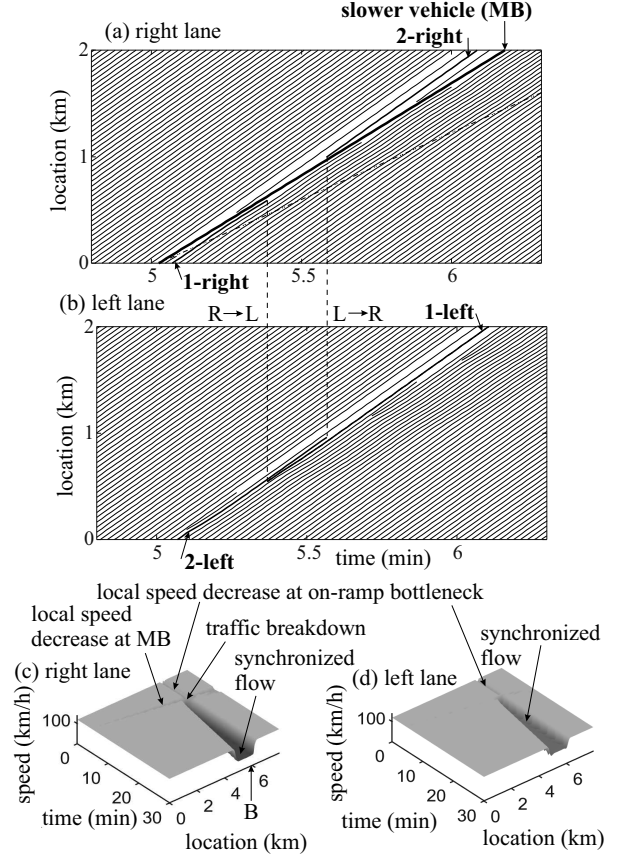


FIG. 13: Simulations of  $F \rightarrow S$  transition occurring due to downstream propagation of MB through the bottleneck that simplified version is shown in Fig. 11 (b): (a, b) Vehicle trajectories in the vicinity of MB in the right lane (a) and left lane (b). (c, d) Speed in space and time in the right lane (c) and left lane (d).  $q_{in} = 2571$  (vehicles/h)/lane,  $q_{on} = 720$  vehicles/h,  $L_M = 0.3$  km. Other model parameters are the same as those in Fig. 3.

## B. Time delay of spontaneous traffic breakdown (spontaneous $F \rightarrow S$ transition)

There is a time delay of the spontaneous  $F \rightarrow S$  transition at the bottleneck denoted by  $T^{(B)}$  (Figs. 15 and 16): Under condition (10), it has been found that the less the difference  $q_{sum} - C_{max}$ , the longer the time delay  $T^{(B)}$  is (Fig. 16). In the time-delay-flow-rate plane, condition  $q_{sum} = C_{max}$  determines an asymptote (dashed vertical line in Fig. 16) that separates metastable free flow (left of the asymptote) and unstable free flow with respect to the  $F \rightarrow S$  transition (right of the asymptote) [139].

## C. Range of discontinuity of over-acceleration rate

Within the flow-rate range (8) there can be either a free flow state or a synchronized flow state at the bottleneck.

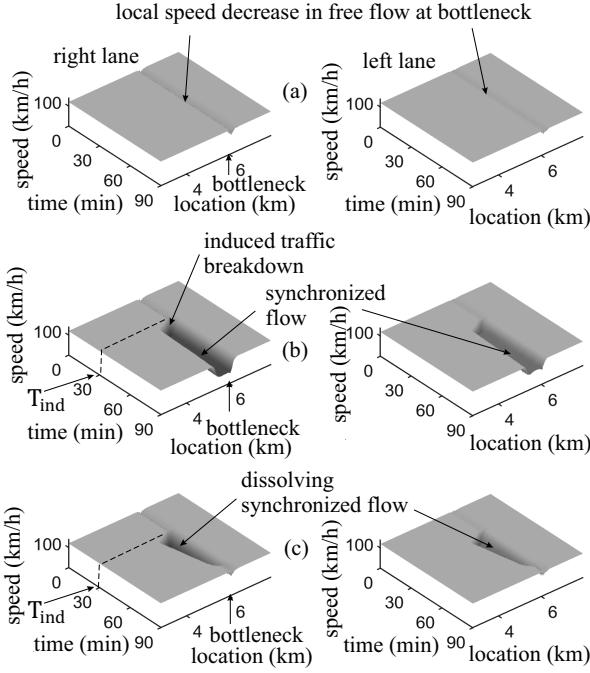


FIG. 14: Simulations of minimum capacity  $C_{\min} = 2q_{\text{in}} + q_{\text{on},\min}$  of free flow at bottleneck. Speed in space and time in the right lane (left column) and in left lane (right column) at different  $q_{\text{on}}$  at the same value  $q_{\text{in}} = 2571$  (vehicles/h)/lane as that in Fig. 3: (a) Free flow. (b) Induced traffic breakdown in (a). (c) Induced dissolving synchronized flow. In (a, b),  $q_{\text{on}} = q_{\text{on},\min} = 650$  vehicles/h, i.e.,  $C_{\min} = 5792$  vehicles/h; in (c),  $q_{\text{on}} = 630$  vehicles/h. In (b, c), as explained in Sec. II B, on-ramp inflow rate impulse has been applied; parameters of the impulse inducing either F $\rightarrow$ S transition (induced traffic breakdown) (b) or dissolving synchronized flow (c) at bottleneck are:  $T_{\text{ind}} = 30$  min,  $\Delta t = 5$  min;  $\Delta q_{\text{on}} = 250$  vehicles/h in (b) and  $\Delta q_{\text{on}} = 270$  vehicles/h in (c). Other model parameters are the same as those in Fig. 3.

Under condition  $q_{\text{in}} = \text{const}$ , the range (8) is equivalent to the on-ramp inflow-rate range (Fig. 17)

$$q_{\text{on},\min} \leq q_{\text{on}} < q_{\text{on},\max}. \quad (11)$$

When the initial state is free flow and  $q_{\text{on}}$  increases, then at  $q_{\text{on}} > q_{\text{on},\max}$  a spontaneous F $\rightarrow$ S transition occurs with a delay time  $T^{(B)}$  (Figs. 15 and 16). The emergent synchronized flow persists due to the discontinuity in the over-acceleration rate (Sec. II D): The over-acceleration rate decreases sharply (down-arrow in Fig. 17 (a)), respectively, the mean time delay in over-acceleration increases sharply (up-arrow in Fig. 17 (b)).

When  $q_{\text{on}}$  decreases, synchronized flow exists in the range (11). Only when  $q_{\text{on}}$  becomes less than  $q_{\text{on},\min}$ , a return spontaneous S $\rightarrow$ F transition occurs at the bottleneck; respectively, free flow recovers at the bottleneck. Thus, there is a Z-characteristic for traffic breakdown at the bottleneck that shows stable, metastable, and unstable states of free flow with respect to the F $\rightarrow$ S transition at the bottleneck (Fig. 17).

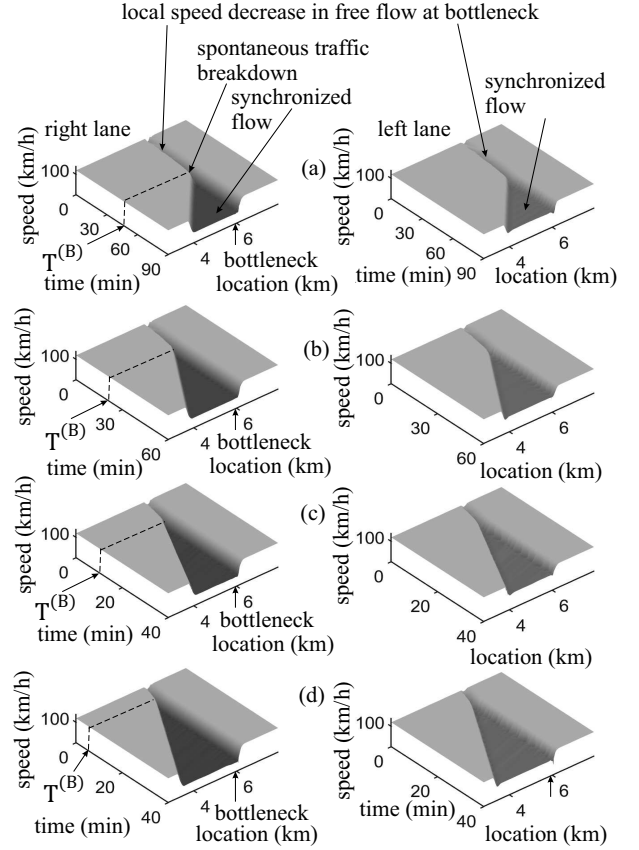


FIG. 15: Simulations of spontaneous F $\rightarrow$ S transition at bottleneck. Speed in space and time in the right lane (left column) and in left lane (right column) at different  $q_{\text{on}}$  at the same value  $q_{\text{in}} = 2571$  (vehicles/h)/lane as that in Fig. 3: (a)  $q_{\text{on}} = 729$  vehicles/h,  $T^{(B)} = 51$  min. (b)  $q_{\text{on}} = 740$  vehicles/h,  $T^{(B)} = 19.8$  min. (c)  $q_{\text{on}} = 760$  vehicles/h,  $T^{(B)} = 10$  min. (d)  $q_{\text{on}} = 780$  vehicles/h,  $T^{(B)} = 5$  min. Other model parameters are the same as those in Fig. 3.

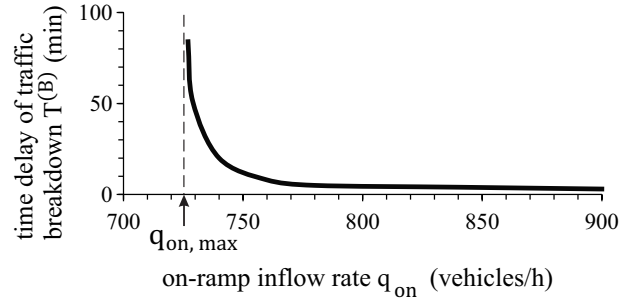


FIG. 16: Continuation of Fig. 15. Dependence of the time delay  $T^{(B)}$  of spontaneous F $\rightarrow$ S transition at bottleneck on on-ramp inflow rate  $q_{\text{on}}$  at the given flow rate  $q_{\text{in}} = 2571$  (vehicles/h)/lane. Calculated values  $q_{\text{on},\max} = 726$  vehicles/h,  $C_{\max} = 2q_{\text{in}} + q_{\text{on},\max} = 5868$  vehicles/h.

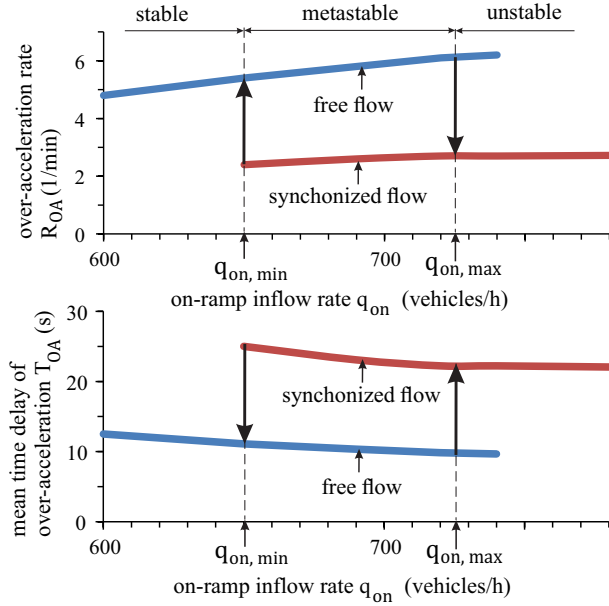


FIG. 17: Simulated range of the discontinuity in over-acceleration rate (a) and in mean time-delay in over-acceleration (b) as functions of the on-ramp inflow rate  $q_{on}$  at given flow rate  $q_{in} = 2571$  (vehicles/h)/lane: Z-characteristics of the F $\rightarrow$ S transition in automated-driving vehicular traffic on two-lane road with bottleneck. Other model parameters are the same as those in Fig. 3.

#### D. Physics of spontaneous traffic breakdown

The spontaneous F $\rightarrow$ S transition occurs at  $t = T^{(B)}$  (Sec. III B) when a *sequence of two R $\rightarrow$ L lane-changing* occurs: One of them is realized at the upstream front of the local speed decrease (vehicle 1 in Figs. 18 (a, b)) and another occurs at its downstream front (vehicle 2 in Figs. 18 (a, b)). Simultaneously, a drop in the over-acceleration rate  $R_{OA}$  (Fig. 18 (c)) and, respectively, a jump in the mean time delay in over-acceleration  $T_{OA}$  are realized (Fig. 18 (d)). As explained in Sec. II D, this discontinuous behavior of over-acceleration causes the abrupt transformation of the local speed decrease in free flow at the bottleneck into synchronized flow. The boundaries of synchronized flow are given by the upstream synchronized flow front propagating upstream (dashed curve “S-up” in Fig. 18 (a, b)) and the downstream synchronized flow front (dashed-dotted curve “S-down”) fixed at the bottleneck.

The physics of the maximum capacity  $C_{max}$  and time delay  $T^{(B)}$  of spontaneous traffic breakdown is as follows. As found, at  $q_{on} < q_{on, max}$  the minimum speed within the local speed decrease in free flow at the bottleneck does not almost depend on time (Fig. 3). Contrarily, at  $q_{on} > q_{on, max}$  (Fig. 15), the minimum speed within the local speed decrease in free flow grows continuously over time. Indeed, at  $t \ll T^{(B)}$  (Fig. 19) minimum speeds of vehicles 3 and 4 are considerably larger than minimum speeds,

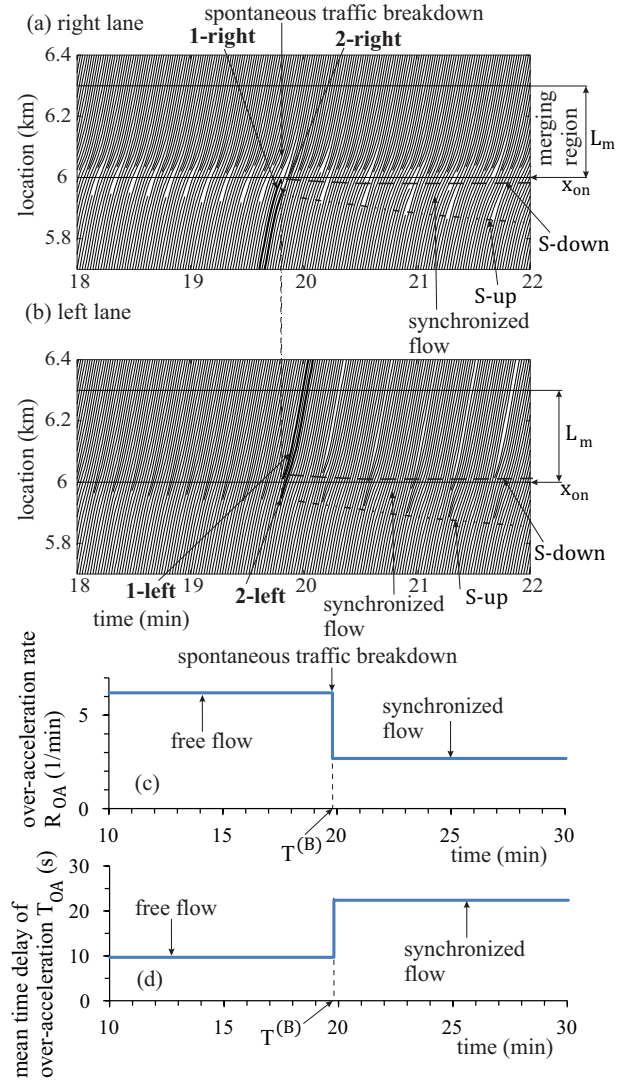


FIG. 18: Continuation of Fig. 15 (b). Features of spontaneous traffic breakdown: (a, b) Vehicle trajectories in the right lane (a) and left lane (b). (c, d) Time-dependencies of the averaged over-acceleration rate  $R_{OA}$  (c) and the mean time delay in over-acceleration  $T_{OA}$  (d).

respectively, of vehicles 5 and 7 moving in free flow at time that is only about 30 s less than  $t = T^{(B)}$  (Figs. 20 (c, d)). Thus, the maximum capacity  $C_{max}$  separates free flow states at  $q_{on} < q_{on, max}$ , in which the local speed decrease at the bottleneck does not growth over time, from free flow states at  $q_{on} > q_{on, max}$ , in which the local speed decrease does continuously grow over time.

The continuous reduction of the minimum speed within the local speed decrease in free flow at the bottleneck over time has to have a limit that can be considered a critical minimum speed: After vehicle “on-3” has merged from the on-ramp, minimum speeds of vehicles 8 and 9 moving in the right lane become low enough; this causes the sequence of two R $\rightarrow$ L lane-changing of vehicles 1 and

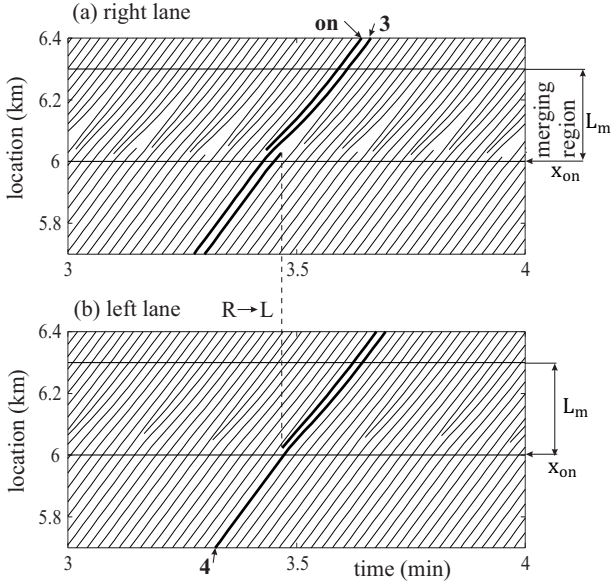


FIG. 19: Continuation of Fig. 15 (b): Vehicle trajectories in free flow at the bottleneck at  $t \ll T^{(B)}$ .

2 (Figs. 21 (a, b)). Slow vehicles 1-left and 2-left (Figs. 21 (c, d)) force the following vehicles 11 and 12 moving in the left lane to decelerate strongly. At so low speed in the left lane the over-acceleration rate  $R_{OA}$  drops and, respectively, the mean time delay in over-acceleration increases sharply (Figs. 18 (c, d)); as a result, the speed adaptation overcomes the over-acceleration.

It takes some time for the continuous reduction of the minimum speed within the local speed decrease to the critical speed in free flow at which traffic breakdown occurs at the bottleneck. This time interval determines the time delay  $T^{(B)}$  of traffic breakdown ( $F \rightarrow S$  transition). We have found that the more the on-ramp inflow rate  $q_{on}$  exceeds the critical value  $q_{on,max}$ , the quicker the critical minimum speed in free flow at the bottleneck is reached. This explains the decreasing character of function  $T^{(B)}(q_{on})$  (Fig. 16).

#### IV. GENERALIZATION OF NUCLEATION FEATURES OF $F \rightarrow S$ TRANSITION IN AUTOMATED-DRIVING TRAFFIC

Up to now we have used only one chosen set of model parameters, to demonstrate that automated-driving traffic does exhibit the basic feature of the three-phase traffic theory – the nucleation character of an  $F \rightarrow S$  transition at the bottleneck. To disclose the physics of this  $F \rightarrow S$  transition, we have studied its features under a change in the on-ramp inflow rate  $q_{on}$  at the bottleneck (Secs. II and III). However, do basic results of this paper about the nucleation character of the  $F \rightarrow S$  transition at the bottleneck and the existence of a range of highway capacities remain in automated-driving vehicular traffic,

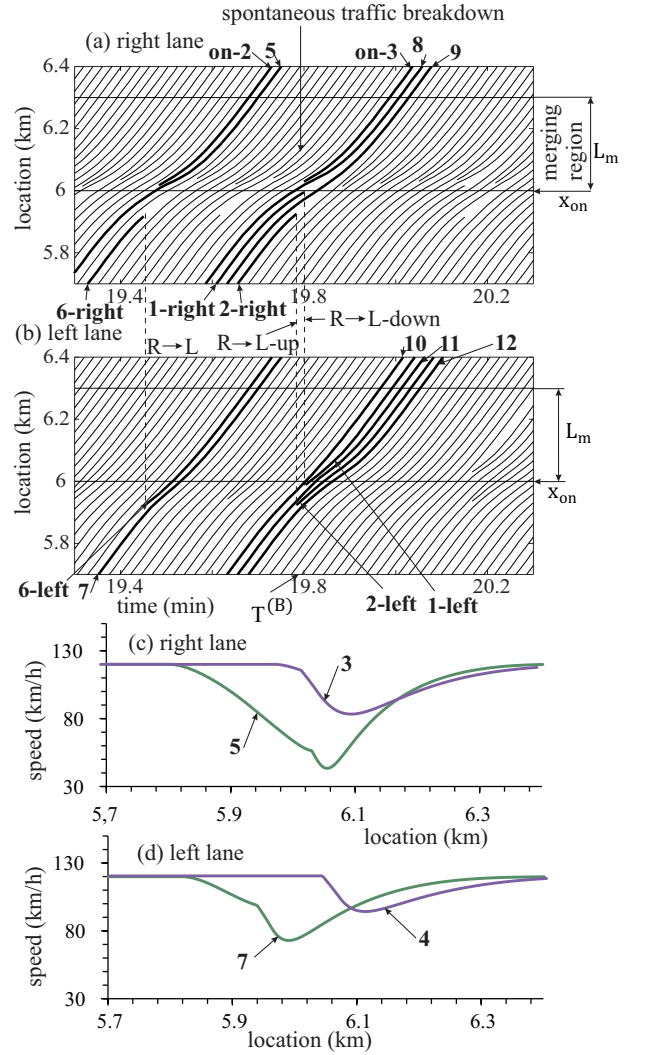


FIG. 20: Continuation of Fig. 15 (b). (a, b) Vehicle trajectories “on-2”, 5–7 are in free flow at time that is about 30 s less than  $t = T^{(B)}$ ; trajectories “on-3”, 8–12 are related to the time of traffic breakdown ( $F \rightarrow S$  transition)  $t = T^{(B)}$ . (c, d) Comparison of location-functions of speeds for vehicles 3 and 4 taken from Fig. 19 with speeds on trajectories 5 and 7 from (a, b). Vehicles 1 and 2 are, respectively, the same as that in Fig. 18 (a, b). Sequence of two  $R \rightarrow L$  lane-changing effects of vehicles 1 and 2 that causes spontaneous traffic breakdown are labeled by  $R \rightarrow L$ -down and  $R \rightarrow L$ -up, respectively.

when model parameters are changed?

##### A. Effect of lane-changing model parameters on $F \rightarrow S$ transition

We have found that as long as new model parameters in lane-changing rules (4)–(6) enable a distribution of on-ramp inflow between road lanes in free flow, all qualitative results presented above remain the same

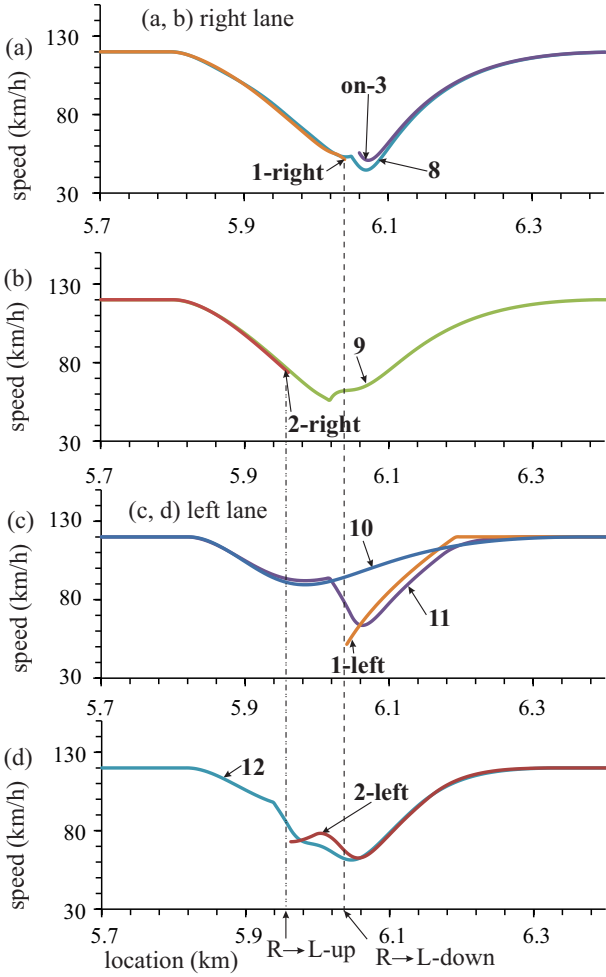


FIG. 21: Continuation of Fig. 20: Location-functions of speed for some vehicles whose numbers are the same as that in Fig. 20, respectively; vehicles 1 and 2 are, respectively, the same as that in Figs. 18 (a, b).

ones. Examples are shown in Fig. 22 for symmetric lane-changing parameters  $\delta_1 = \delta_2$  in (4), (5) (Fig. 22 (a)) and for symmetric safety parameters  $\tau_1 = \tau_2$  in (6).

### B. Diagrams of F→S transition at bottleneck

To understand the nucleation nature of the F→S transition in automated-driving traffic, up to now we have used only one given flow rate in free flow upstream of the bottleneck  $q_{in} = 2571$  (vehicles/h)/lane. We have found that the nucleation nature of the F→S transition at the bottleneck remains when  $q_{in}$  changes (Fig. 23). In particular, maximum capacity  $C_{max}$  does not almost depend on  $q_{on}$ , whereas minimum capacity  $C_{min}$  is a decreasing function of  $q_{on}$ : the larger the on-ramp inflow rate  $q_{on}$ , the larger the capacity range  $C_{max} - C_{min}$  (Fig. 23 (c)). When the flow rate  $q_{on}$  increases, the flow-rate range  $q_{on,max} - q_{on,min}$ , within which free flow

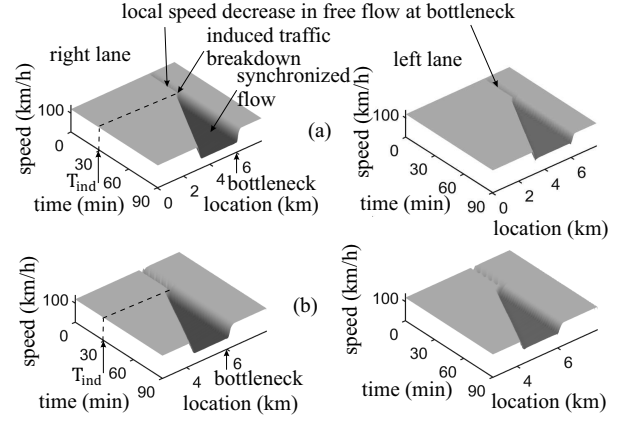


FIG. 22: Speed in space and time in the right lane (left column) and in left lane (right column) at the same flow rate  $q_{in} = 2571$  (vehicles/h)/lane as that in Fig. 3. (a, b) Induced S→J transition that has been simulated as that in Fig. 4. (a) Symmetric lane-changing parameters  $\delta_1 = \delta_2 = 1$  m/s in (4), (5),  $q_{on} = 720$  vehicles/h,  $\Delta q_{on} = 180$  vehicles/h. (b) Symmetric safety parameters  $\tau_1 = \tau_2 = 0.4$  s in (6),  $q_{on} = 700$  vehicles/h,  $\Delta q_{on} = 200$  vehicles/h.  $T_{ind} = 30$  min,  $\Delta t = 2$  min. Other model parameters are the same as those in Fig. 3.

is metastable with respect to the F→S transition at the bottleneck, increases (Fig. 23 (d)).

At any value  $q_{in}$ , at which the F→S transition can occur, the physics of the F→S transition is qualitatively the same as that disclosed in Secs. II and III. In particular, the nature of the F→S transition is caused by the discontinuity of the over-acceleration rate (Fig. 24 (a, b)) as well as its competition with speed adaptation. Features of synchronized flow occurring due to the F→S transition (Sec. II E) remain also the same when  $q_{in}$  changes. The speeds in synchronized flow in the right and left lanes at the bottleneck are decreasing functions of the on-ramp inflow rate (Fig. 24 (c)).

### C. Lane-asymmetric nucleation of F→S transition

Because the nucleation nature of F→S transition in automated-driving traffic at the bottleneck is determined by the existence of the discontinuity in R→L lane-changing rate (Sec. II), a question can arise: Does the nucleation nature of F→S transition remain if the lane-changing rules are changed qualitatively? Indeed, as known, cooperative driving in automated-driving traffic could permit the realization of different lane-changing rules that enable a distribution of on-ramp inflow between road lanes in free flow as done through lane-changing rules (4)–(6). In (4)–(6), at a large speed difference between lanes no speed limitation for lane-changing has been assumed. When a vehicle moving at a slow speed  $v(t)$  changes from the right lane to the left lane, the vehicle can force the following vehicle moving

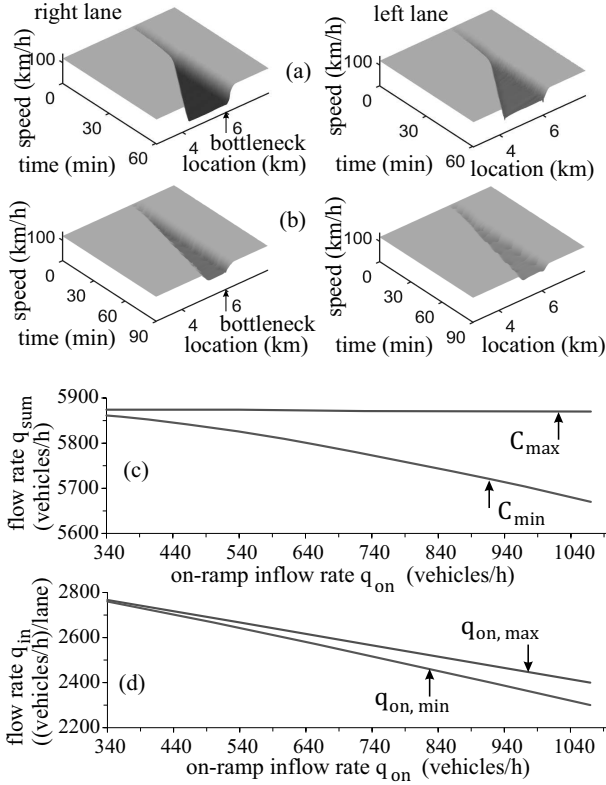


FIG. 23: Simulations of the nucleation nature of the  $F \rightarrow S$  transition at the bottleneck for different values  $q_{in}$ : (a, b) Speed in space and time in the right lane (left column) and in left lane (right column) for spontaneous  $F \rightarrow S$  transition: (a)  $q_{in} = 2449$  (vehicles/h)/lane,  $q_{on} = 980$  vehicles/h,  $T^{(B)} = 26$  min. (b)  $q_{in} = 2769$  (vehicles/h)/lane,  $q_{on} = 340$  vehicles/h,  $T^{(B)} = 24$  min. (c) Dependencies of minimum highway capacity  $C_{min}$  and maximum highway capacity  $C_{max}$  on  $q_{on}$ . (d) Dependencies  $q_{in}(q_{on})$  related to  $C_{min}(q_{on})$  (curve denoted by  $q_{on,min}$ ) and  $C_{max}(q_{on})$  (curve denoted by  $q_{on,max}$ ), respectively. Other model parameters are the same as those in Fig. 3.

at a larger speed  $v^-(t)$  to decelerate strongly. This can considerably decrease comfortable driving and sometimes traffic safety.

Cooperative driving can solve this problem through some safety condition

$$g^-(t) + (v(t) - v^-(t))T_p > g_p \quad (12)$$

used in addition to (6). Safety condition (12), in which  $T_p$  and  $g_p$  are constant parameters, limits  $R \rightarrow L$  lane-changing, when speed difference  $v(t) - v^-(t)$  is large enough, whereas the space gap between these vehicles is not large enough for comfortable driving.

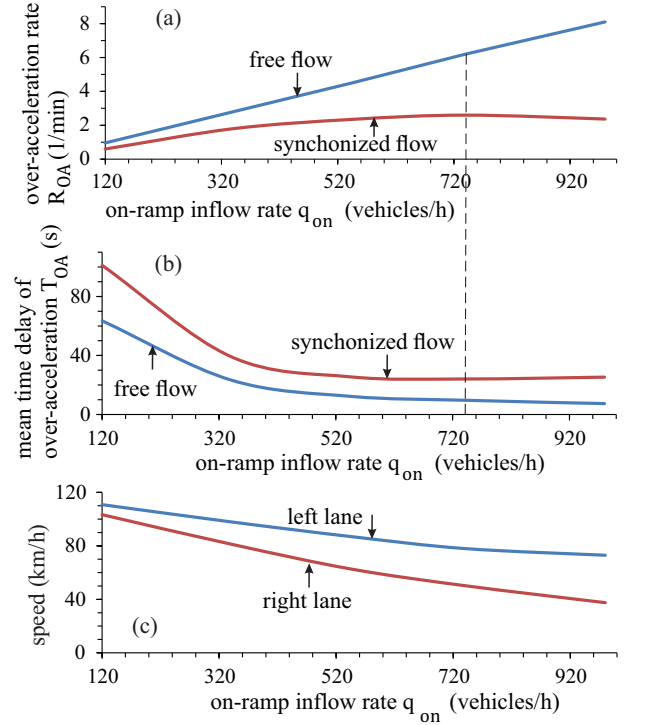


FIG. 24: Characteristics of spontaneous  $F \rightarrow S$  transition at different flow rates  $q_{in}$  in free flow upstream of bottleneck. (a, b) The discontinuity of the over-acceleration rate: On-ramp inflow-rate dependence of the over-acceleration rate  $R_{OA}$  (a) and the mean time delay in over-acceleration  $T_{OA}$  (b) in initial free flow (curves “free flow”) and in synchronized flow (curves “synchronized flow”) that has occurred due to  $F \rightarrow S$  transition. (c) Synchronized flow speeds occurring at the bottleneck after the  $F \rightarrow S$  transition in the right and left lanes. In (a, b), on-ramp inflow-rates  $q_{on}$  on the x-axis are slightly exceed corresponding values  $q_{on,max}$  (we have used  $q_{on} = q_{on,max} + \delta q$ , where parameter  $\delta q = 14$  vehicles/h) calculated by different values  $q_{in}$ ; for explanations of (a, b), a dashed vertical line related to  $q_{on} = 740$  vehicles/h has been drawn to show, respectively, the same values  $R_{OA}$  and  $T_{OA}$  at curves  $R_{OA}(q_{on})$  and  $T_{OA}(q_{on})$  as those in Figs. 18 (c, d) for  $q_{in} = 2571$  (vehicles/h)/lane. Other model parameters are the same as those in Fig. 3.

### 1. Characteristics of lane-asymmetric nucleation of $F \rightarrow S$ transition

Condition (12) does not affect on  $R \rightarrow L$  lane-changing in *free flow* (Fig. 25 (a)): The same lane-changing rate is realized and the same local speed decrease appears at the bottleneck as that in Fig. 3. There is free flow metastability with respect to the  $F \rightarrow S$  transition at the bottleneck as found in Secs. II and III; condition (8) is also valid. Moreover, values  $q_{on,max}$  and, respectively,  $C_{max} = 2q_{in} + q_{on,max}$ , which separate metastable free flow from unstable free flow with respect to the  $F \rightarrow S$  transition at the bottleneck remains almost the same (Figs. 25–27).

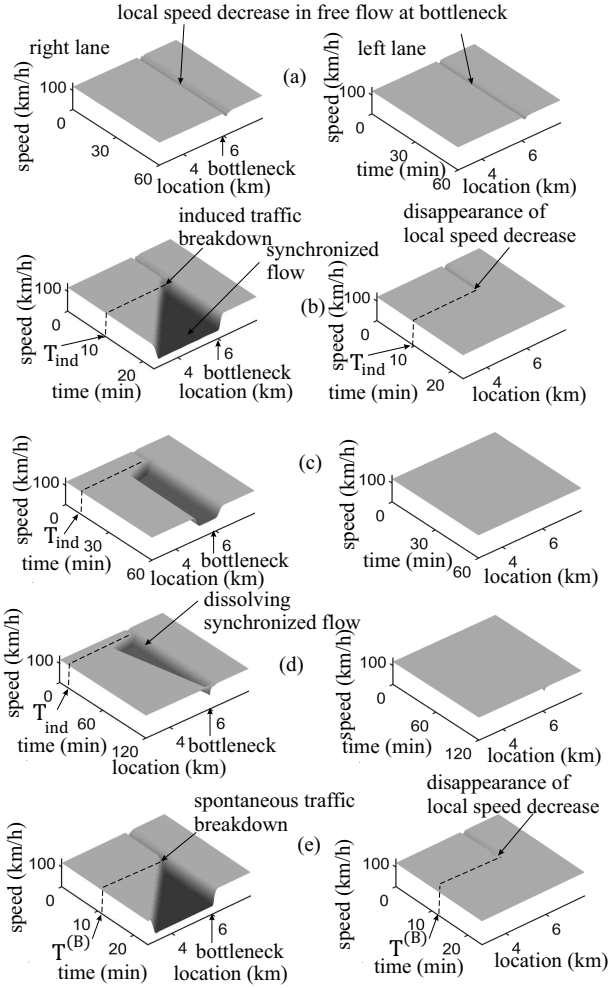


FIG. 25: Simulations of asymmetric  $F \rightarrow S$  transition at bottleneck that occurs in model of Sec. II A, when, in addition to safety conditions (6), condition (12) is used. Speed in space and time in the right lane (left column) and in left lane (right column) at different  $q_{on}$  at the same flow rate  $q_{in} = 2571$  (vehicles/h)/lane as that in Fig. 3: (a) Local speed decrease at bottleneck in free flow,  $q_{on} = 720$  vehicles/h. (b) Induced  $F \rightarrow S$  transition in free flow of (a); parameters of on-ramp inflow impulse:  $T_{ind} = 10$  min,  $\Delta q_{on} = 180$  vehicles/h,  $\Delta t = 1$  min. (c) Induced  $F \rightarrow S$  transition at  $q_{on} = q_{on,min} = 360$  vehicles/h;  $T_{ind} = 10$  min,  $\Delta q_{on} = 540$  vehicles/h,  $\Delta t = 2$  min. (d) Dissolving synchronized flow at  $q_{on} = 350$  vehicles/h that is less than  $q_{on,min}$ ;  $T_{ind} = 10$  min,  $\Delta q_{on} = 550$  vehicles/h,  $\Delta t = 2$  min. (e) Spontaneous  $F \rightarrow S$  transition at  $q_{on} = 727$  vehicles/h that is larger than  $q_{on,max} = 724$  vehicles/h;  $T^{(B)} = 11.5$  min. In (12),  $T_p = 3.3$  s,  $g_p = 2$  m. Other model parameters are the same as those in Fig. 3.

However, the use of condition (12) changes basically the result of the  $F \rightarrow S$  transition at the bottleneck: In Sec. II, after the  $F \rightarrow S$  transition has occurred, synchronized flow emerges both in the right and in left lanes (Figs. 4 and 15). Contrarily, under condition (12) the  $F \rightarrow S$  transition causes synchronized flow emergence in the right lane *only* (Figs. 25 (b–e)). For this reason,

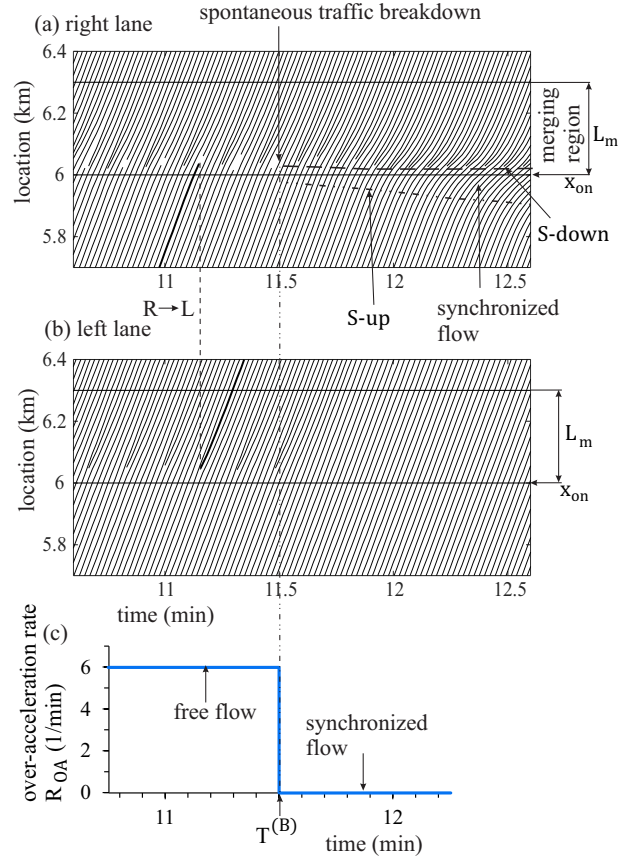


FIG. 26: Continuation of Fig. 25 (e): Features of asymmetric spontaneous traffic breakdown: (a, b) Vehicle trajectories in the right lane (a) and left lane (b). (c) Time-dependencies of the averaged over-acceleration rate  $R_{OA}$ .

we can call the  $F \rightarrow S$  transition as an *asymmetric*  $F \rightarrow S$  transition at the bottleneck.

Moreover, after the asymmetric  $F \rightarrow S$  transition has occurred *no* local speed decrease remains in free flow in the left lane at the bottleneck (right column in Figs. 25 (b–e)). The disappearance of the local speed decrease in free flow in the left lane at the bottleneck is explained by the drop in the  $R \rightarrow L$  lane-changing rate to zero during the asymmetric  $F \rightarrow S$  transition (Fig. 26): No  $R \rightarrow L$  lane-changing is realized at  $t > T^{(B)}$ , i.e., after the asymmetric  $F \rightarrow S$  transition has occurred at  $t = T^{(B)}$  (Fig. 26 (a, b)). Respectively, there is a drop in the over-acceleration rate  $R_{OA}$  from the rate  $R_{OA}$  in free flow to  $R_{OA} = 0$  in synchronized flow (Fig. 26 (c)); one of these  $R \rightarrow L$  lane-changing at  $t < T^{(B)}$  is marked by dashed vertical line  $R \rightarrow L$  in Figs. 26 (a, b) [140]. The physics of this effect is as follows. When synchronized flow begins to emerge in the right lane, the speed difference  $v(t) - v^-(t)$  in (12) becomes large enough. This prevents the  $R \rightarrow L$  lane-changing.

We have found that as in Fig. 16, time delay  $T^{(B)}$  of spontaneous asymmetric  $F \rightarrow S$  transition that occurs at  $q_{on} > q_{on,max}$  is also a strongly falling on-ramp



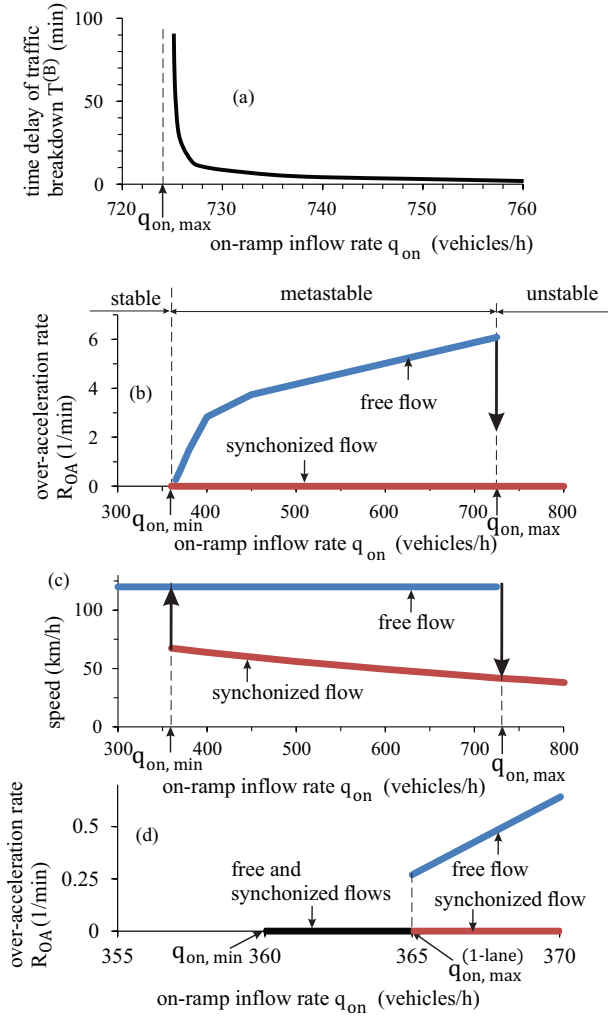


FIG. 27: Simulated characteristics of asymmetric  $F \rightarrow S$  transition on two-lane road with bottleneck at the same value  $q_{in} = 2571$  (vehicles/h)/lane as that in Figs. 3–10. (a) Dependence of time delay  $T^{(B)}$  of spontaneous traffic breakdown on  $q_{on}$ ;  $q_{on,max} = 724$  vehicles/h,  $C_{max} = 2q_{in} + q_{on,max} = 5868$  vehicles/h. (b, c) Simulated Z-characteristics of the asymmetric  $F \rightarrow S$  transition: The discontinuity in over-acceleration rate (b) and speed (c) as functions of  $q_{on}$ . (d) A small part of (b) in a large scale in vicinity of  $q_{on} = q_{on,min}$ . Other model parameters are the same as those in Fig. 25.

inflow-rate function (Fig. 27 (a)). However, under the asymmetric  $F \rightarrow S$  transition there is a considerable reduction in values  $q_{on,min}$  and, respectively,  $C_{min} = 2q_{in} + q_{on,min}$  (Figs. 27 (b, c)) in comparison with these values found in Sec. III (Fig. 14). Other peculiarities of the asymmetric  $F \rightarrow S$  transition have been found when  $q_{on}$  decreases: (i) The value  $R_{OA}$  decreases strongly (Fig. 27 (b)). (ii) The discontinuity in the over-acceleration rate  $R_{OA}$  remains until some inflow-rate denoted by  $q_{on,max}^{(1-lane)}$  that slightly exceeds  $q_{on,min}$  (Fig. 27 (d)). (iii) Although within a range

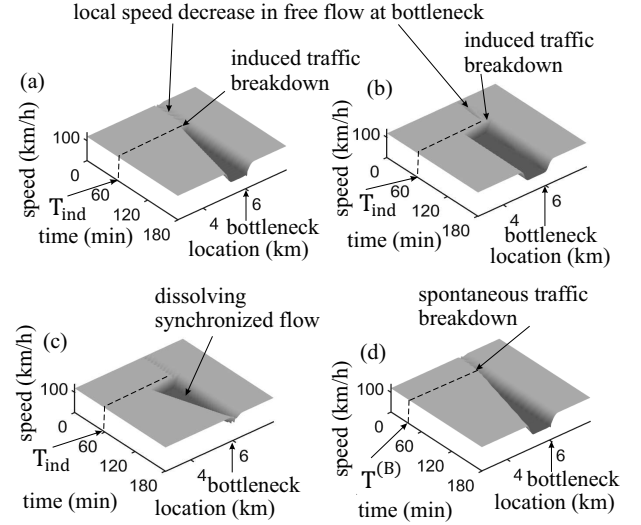


FIG. 28: Simulations of  $F \rightarrow S$  transition on single-lane road with bottleneck model of Sec. II A. Speed in space and time at different  $q_{on}$  at the same value  $q_{in} = 2571$  vehicles/h as that in Fig. 3: (a) Induced traffic breakdown in metastable free flow at  $q_{on} = 365$  vehicles/h,  $T_{ind} = 60$  min,  $\Delta q_{on} = 135$  vehicles/h,  $\Delta t = 1$  min; (b) Induced traffic breakdown in metastable free flow at  $q_{on} = 360$  vehicles/h,  $T_{ind} = 60$  min,  $\Delta q_{on} = 540$  vehicles/h,  $\Delta t = 2$  min; (c) Dissolving synchronized flow at  $q_{on} = 350$  vehicles/h,  $T_{ind} = 60$  min,  $\Delta q_{on} = 550$  vehicles/h,  $\Delta t = 2$  min; (d) Time-delayed spontaneous traffic breakdown at  $q_{on} = 366$  vehicles/h,  $T^{(B)} = 30$  min.  $q_{on,min} = 360$  vehicles/h,  $q_{on,max}^{(1-lane)} = 365.2$  vehicles/h. Other model parameters are the same as those in Fig. 3.

$q_{on,min} \leq q_{on} < q_{on,max}^{(1-lane)}$  free flow is still metastable with respect to the asymmetric  $F \rightarrow S$  transition, nevertheless, the discontinuity in the over-acceleration rate  $R_{OA}$  does not exist any more: there is no lane-changing within the inflow-rate range  $q_{on,min} \leq q_{on} < q_{on,max}^{(1-lane)}$  at all. To understand this result, we consider in Sec. IV C 2 automated-driving traffic on a single-lane road with the same bottleneck.

## 2. Over-acceleration in automated-driving traffic on single-lane road

After the asymmetric  $F \rightarrow S$  transition has occurred, *no* effect of the bottleneck on the vehicle motion in the left lane is realized any more (right column in Figs. 25 (b–e)); therefore, each of the road lanes could be considered as two different (and not connected) single-lane roads.

We have found that although no  $R \rightarrow L$  lane-changing is possible on the single-lane road, within the range  $q_{on,min} \leq q_{on} < q_{on,max}^{(1-lane)}$  free flow is indeed in a metastable state with respect to the  $F \rightarrow S$  transition at the bottleneck (Fig. 28 (a–c)). The maximum on-ramp inflow-rate  $q_{on,max}^{(1-lane)}$  determines the maximum capacity

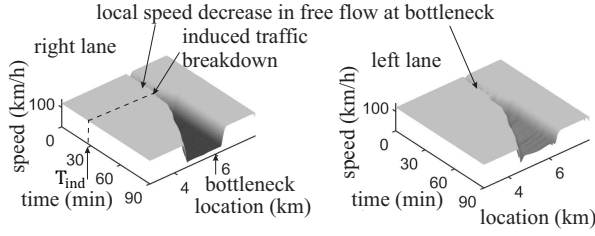


FIG. 29: Simulations of the effect of the increase in desired time headway  $\tau_d$  of automated vehicles on nucleation features of  $F \rightarrow S$  transition with the model of Sec. II A on two-lane road with bottleneck: Speed in space and time in the right lane (left) and in left lane (right). Induced traffic breakdown under condition (8).  $\tau_d = 1.5$  s with  $K_1 = 0.3$  s $^{-2}$ ,  $K_2 = 0.6$  s $^{-1}$  in (1), (2),  $\tau_1 = \tau_2 = 0.9$  s in (6),  $q_{in} = 1714$  (vehicles/h)/lane,  $q_{on} = 710$  vehicles/h,  $T_{ind} = 30$  min,  $\Delta q_{on} = 190$  vehicles/h,  $\Delta t = 2$  min. Other model parameters are the same as those in Fig. 3.

of automated-driving traffic on the single-lane road with the bottleneck:  $C_{max} = q_{in} + q_{on,max}^{(1-lane)}$ : At a given  $q_{in}$ , when  $q_{on} > q_{on,max}^{(1-lane)}$  after a time delay  $T^{(B)}$ , which is a decreasing on-ramp inflow-rate function, the  $F \rightarrow S$  transition occurs spontaneously at the bottleneck (Fig. 28 (d)).

Thus, the minimum on-ramp inflow-rate  $q_{on,min}$  of free flow metastability with respect to the asymmetric  $F \rightarrow S$  transition at the bottleneck on two-lane road is determined by the minimum on-ramp inflow-rate  $q_{on,min}$  of free flow metastability on single-lane road with the same bottleneck. To explain this result, we should recall that in three-phase traffic theory [93–95], the term *over-acceleration* determines driver acceleration behaviors associated with a time delay in acceleration that causes free flow metastability with respect to an  $F \rightarrow S$  transition at a bottleneck. In Helly’s model (1), (2) there is a time delay in acceleration. For this reason, it is not surprising that Helly’s model (1), (2) shows over-acceleration on the single-lane road. However, the effect of this over-acceleration is practically insignificant: the range of the free flow metastability on single-lane road is only  $q_{on,max}^{(1-lane)} - q_{on,min} = 5$  vehicles/h (Fig. 27 (d)) [141].

#### D. Effect of desired time headway of automated vehicles

The basic result about the metastability of free flow with respect to the  $F \rightarrow S$  transition at the bottleneck remains under a wide range of the desired time headway  $\tau_d$  of automated vehicles. However, as shown in Fig. 29, the increase in  $\tau_d$  to 1.5 s leads to a considerable decrease in the flow rate  $q_{in}$  at which the metastability of free flow is realized.

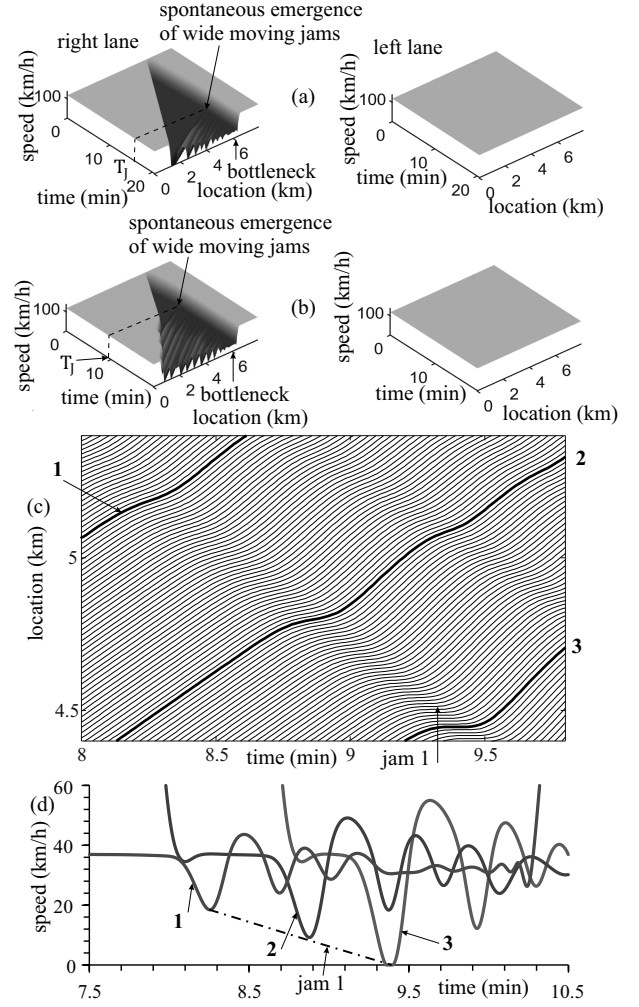


FIG. 30: Simulations of spontaneous  $S \rightarrow J$  transition in model of Sec. IV C with the use of (13). Speed in space and time in the right lane (left column) and in left lane (right column) at different  $q_{on}$  at the same flow rate  $q_{in} = 2571$  (vehicles/h)/lane as that in Fig. 3: (a)  $q_{on} = 900$  vehicles/h; (b)  $q_{on} = 940$  vehicles/h. (c) Vehicle trajectories in the right lane for a part of (b). (d) Time-functions of speeds of vehicles 1, 2, and 3 shown in (c). In (13),  $v_{min} = 36$  km/h,  $g_{min} = 3$  m. Other model parameters are the same as those in Fig. 25.

## V. TRANSITIONS BETWEEN THE THREE PHASES IN AUTOMATED-DRIVING VEHICULAR TRAFFIC

Wide moving jams can emerge in synchronized flow. We have found that features of the jams are qualitatively almost the same as well-known for human-driving traffic. Thus, we present a simplified analysis of wide moving jams for model of Sec. IV C, when due to the use of condition (12) synchronized flow and wide moving jams can emerge in the right road lane only.

For a study of very low speed states in automated-driving vehicular traffic, we should note

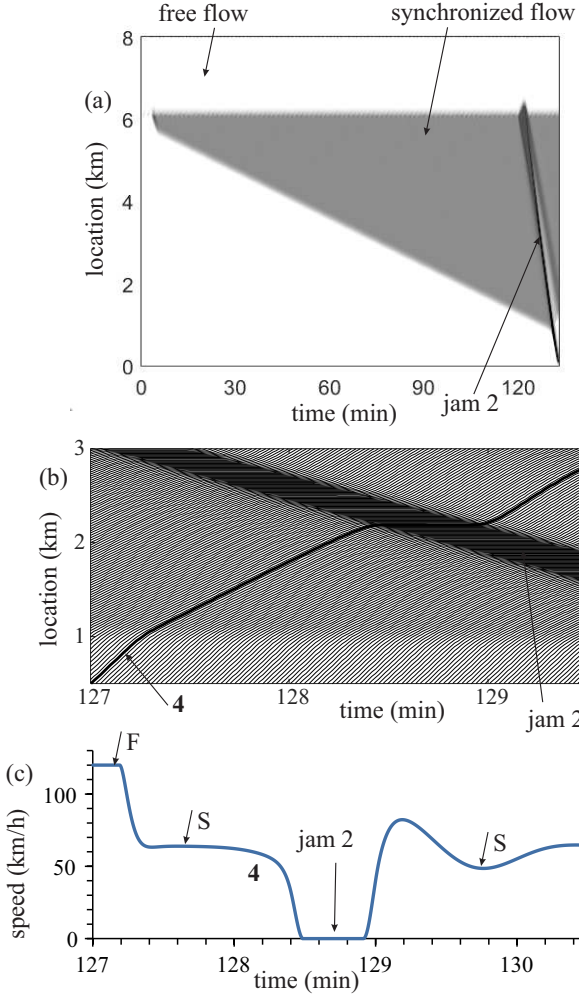


FIG. 31: Simulations of coexistence of the three phases F, S, and J with the use of a sequence of induced F→S and S→J transitions in model of Sec. IV C with the use of (13) at the same flow rate  $q_{in} = 2571$  (vehicles/h)/lane as that in Fig. 3. (a) Speed data in space and time in the right lane presented by regions with variable shades of gray [shades of gray vary from white to black when the speed decreases from 120 km/h (white) to 0 km/h (black)].  $q_{on} = 400$  vehicles/h; for induced F→S transition,  $T_{ind} = 3$  min,  $\Delta q_{on} = 500$  vehicles/h,  $\Delta t = 1$  min; for induced S→J transition,  $T_{ind} = 120$  min,  $\Delta q_{on} = 800$  vehicles/h,  $\Delta t = 2$  min. (b) Vehicle trajectories in the right lane for a part of (a). (c) Time-function of speed of vehicle 4 in (b). Wide moving jam (J) is marked by “jam 2”, F – free flow, S – synchronized flow. Other model parameters are the same as those in Fig. 30.

that in Eq. (1), when the speed  $v \rightarrow 0$ , the optimal gap between vehicles  $g_{opt}$  (2) tends also to zero:  $g_{opt} \rightarrow 0$ . However, even when all vehicles are in standstill, the space gap between vehicles should be larger than zero. Therefore, when the vehicle speed decreases below some low speed denoted by  $v_{min}$ , in formula (2) we should add some additional space gap denoted by  $g_{min}$  to which the space gap  $g$  between automated vehicles tends when

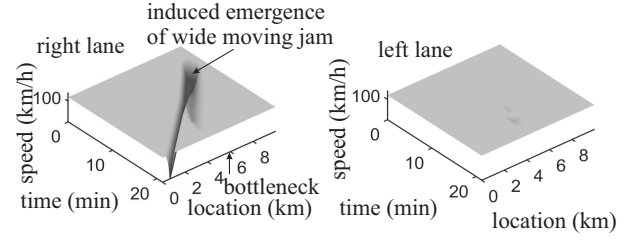


FIG. 32: Simulations of induced F→J transition in model of Sec. IV C with condition (13). Speed in space and time in the right lane (left column) and in left lane (right column) at  $q_{in} = 2880$  (vehicles/h)/lane and  $q_{on} = 0$ ; for induced F→J transition,  $T_{ind} = 3$  min,  $\Delta q_{on} = 1200$  vehicles/h,  $\Delta t = 2$  min. Other model parameters are the same as those in Fig. 30.

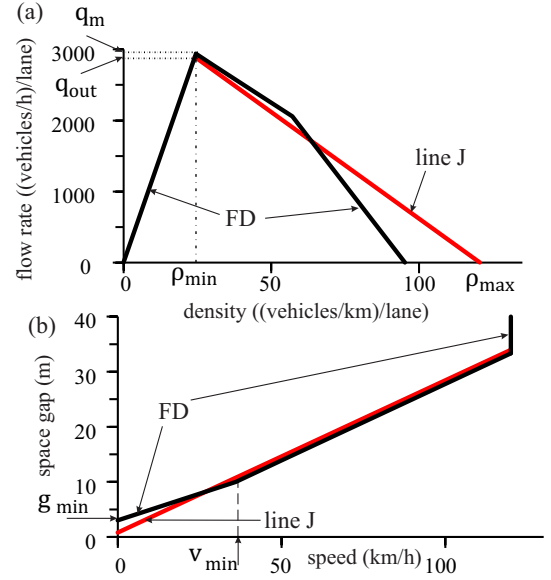


FIG. 33: Fundamental diagrams for hypothetical steady states (curves FD) and line J in the flow–density plane (a) and in the space-gap–speed plane (b). Model of Sec. IV C with the use of (13). The maximum flow rate on FD is  $q_m = 3600/(\tau_d + (d/v_{free})) = 2939$  (vehicles/h)/lane. Characteristics of line J calculated for the wide moving jam in Fig. 32 during the jam propagation in free flow are  $v_g = 30$  km/h,  $q_{out} = 2893$  (vehicles/h)/lane,  $\rho_{min} = 24.5$  (vehicles/km)/lane,  $\rho_{max} = 120.6$  (vehicles/km)/lane. Other model parameters are the same as those in Fig. 30.

the speed  $v \rightarrow 0$ ; therefore, formula (2) is replaced by a known formula

$$g_{opt} = \begin{cases} v\tau_d & \text{at } v \geq v_{min}, \\ g_{min} + v(\tau_d - \tau_{min}) & \text{at } v < v_{min}, \end{cases} \quad (13)$$

where  $\tau_{min} = g_{min}/v_{min}$ ;  $g_{min}$  and  $v_{min}$  are constants.

We have found that in automated-driving traffic either a spontaneous S→J transition (Fig. 30) or induced S→J transition (Fig. 31) can be realized. Vehicle

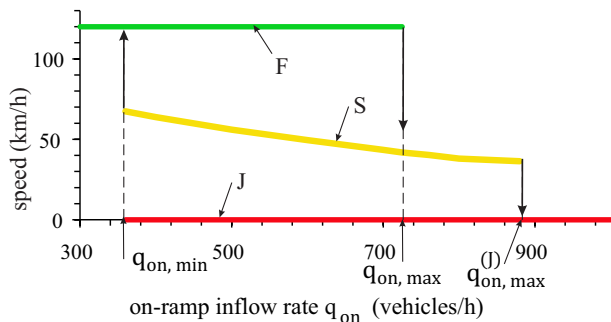


FIG. 34: Double Z (2Z)-characteristic for transitions between the three phases F, S, and J: On-ramp inflow-rate function of average speed within the phases F, S, and J. Model of Sec. IV C with the use of (13) at  $q_{in} = 2571$  (vehicles/h)/lane of Fig. 3.  $q_{on,max}^{(J)} = 880$  vehicles/h. Other model parameters are the same as those in Figs. 27 and 30.

trajectories 1, 2, and 3 in Figs. 30 (c, d) show a typical example of a time-development of an emergent wide moving jam (marked by “jam 1”) during the spontaneous S→J transition. The dynamics of the induced S→J transition (Fig. 31 (a, b)) as well as a time-dependence of the speed of vehicle 4 propagating through the induced wide moving jam (marked by “jam 2”) show a possible coexistence of all three phases F, S, and J in automated-driving traffic (Fig. 31 (c)) that is qualitatively very similar to that known for human-driving traffic. In addition with S→J transitions, a wide moving jam can be induced in free flow (induced F→J transition) (Fig. 32).

As in human-driving traffic, there are characteristics parameters of the downstream front propagation of a wide moving jam in automated-driving traffic that do not depend on initial conditions. The characteristic jam parameters presented by a line J in Fig. 33 are: (i) the velocity of the upstream propagation of the downstream jam front  $v_g$ , (ii) the flow rate  $q_{out}$  and (iii) the density  $\rho_{min}$  in the jam outflow (when free flow is built in this jam outflow) as well as (iv) the density within the jam  $\rho_{max}$ .

States of free flow, synchronized flow, and wide moving jams build together a double-Z (2Z)-characteristic for phase transitions in automated-driving traffic (Fig. 34). At a given  $q_{in}$ , there is some maximum on-ramp inflow-rate  $q_{on}$  denoted by  $q_{on,max}^{(J)}$  (Fig. 34). The condition  $q_{on} = q_{on,max}^{(J)}$  separates metastable synchronized flow at  $q_{on} \leq q_{on,max}^{(J)}$  and unstable synchronized flow at  $q_{on} > q_{on,max}^{(J)}$ , when after a time delay  $T_J$  a spontaneous S→J transition is realized (Fig. 30). The larger the difference  $q_{on,max}^{(J)} - q_{on}$ , the shorter the time delay  $T_J$  of the S→J transition (Figs. 30 (a, b)).

The 2Z-characteristic shows (Fig. 34) that any phase transitions between the three phases F, S, and J

are possible in a broad range of the flow rate in automated-driving vehicular traffic on two-lane road at the bottleneck.

## VI. DISCUSSION

We have shown that traffic on a two-lane road with a bottleneck that consists of 100% string-stable automated vehicles moving in a road lane in accordance with the classical Helly’s model [126] is described in the framework of the three-phase traffic theory in which traffic breakdown is an F→S transition that exhibits the nucleation nature. Does this basic paper result remain when vehicle platoons are string-unstable (Sec. VI A) or when a qualitatively different model for automated-driving vehicles is used (Sec. VI B)?

### A. F→S transition at bottleneck in automated-driving vehicular traffic under string-unstable conditions

The basic paper result about the nucleation nature of traffic breakdown (F→S transition) of the three-phase traffic theory is valid for both string-stable and string-unstable automated-driving vehicular traffic (Fig. 35). In free flow, when the speed is equal to  $v_{free}$ , the mean time headway between vehicles is longer than the desired value  $\tau_d$  in (1), (2). Therefore, no long enough vehicle platoons in which automated vehicles moves at time headway  $\tau_d$  can be built in free flow at the bottleneck: No string instability does occur in free flow. This explains why basic features of the free flow metastability with respect to the F→S transition at the bottleneck remain qualitatively the same as those found in Secs. II–V for string-stable automated vehicles.

Contrary to free flow, in synchronized flow resulting from the F→S transition at the bottleneck very long vehicle platoons in which automated vehicles moves at time headway  $\tau_d$  can be built. For this reason, in synchronized flow the string instability is realized (Fig. 36). However, a detailed study of the development of the string instability in synchronized flow that could be an interesting subject of scientific investigations is out of scope of this paper.

### B. Automated-driving traffic based on three-phase adaptive cruise control (TPACC)

The basic result of the paper about the nucleation nature of traffic breakdown (F→S transition) of the three-phase traffic theory remains when a qualitatively different model for automated-driving vehicles is used. In Fig. 37, automated-driving traffic based on three-phase adaptive cruise control (TPACC) is simulated. The

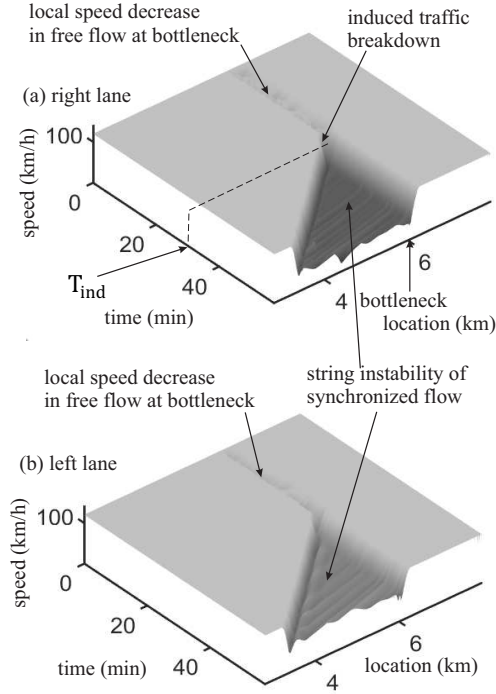


FIG. 35: Simulations of  $F \rightarrow S$  transition on two-lane road with bottleneck of model of Sec. II A with the use of (13), however, when condition (3) for string stability is *not* satisfied: Speed in space and time in the right lane (left) and in left lane (right) at  $q_{in} = 2571$  (vehicles/h)/lane of Fig. 3. Induced  $F \rightarrow S$  transition simulated as in Fig. 4.  $\tau_d = 1$  s,  $K_1 = 0.3$  s $^{-2}$ ,  $K_2 = 0.75$  s $^{-1}$ ,  $q_{on} = 650$  vehicles/h,  $T_{ind} = 30$  min,  $\Delta q_{on} = 250$  vehicles/h,  $\Delta t = 2$  min. Other model parameters are the same as those in Fig. 3.

TPACC-model reads as follows [125, 129]:

$$a^{(TPACC)} = \begin{cases} K_{\Delta v} \Delta v & \text{at } g_{safe} \leq g \leq G, \\ K_1(g - g_{opt}) + K_2 \Delta v & \text{at } g < g_{safe} \text{ or } g > G, \end{cases} \quad (14)$$

where  $K_{\Delta v}$  is a constant dynamic coefficient ( $K_{\Delta v} > 0$ ),  $g_{opt}$  is given by (13) when in this formula  $\tau_d$  is replaced by model parameter  $\tau_p$  that satisfies condition  $\tau_p < \tau_G$ ,  $\tau_G$  is a synchronization space gap;  $g_{safe} = v\tau_{safe}$ ,  $\tau_{safe}$  is a safe time headway. In contrast with the model (1), (13), in the TPACC-model (14) there is an indifference zone for car-following when time headway is between  $\tau_{safe}$  and  $\tau_G$ , i.e., there is no fixed desired time headway between vehicles in TPACC-vehicle platoons. For this reason, as shown in [125], there is no string-instability in TPACC-vehicle platoons.

Simulations show that nucleation features of the  $F \rightarrow S$  transition in automated-driving based on the TPACC-model (14) are qualitatively the same as those found in Secs. II–V for string-stable automated vehicular traffic with the use of Helly’s model (1), (2). However, there are some qualitative differences in

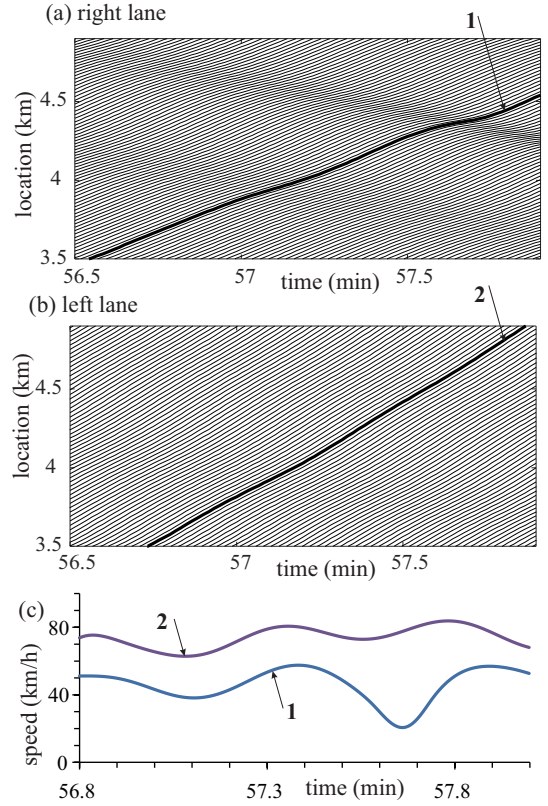


FIG. 36: Continuation of Fig. 35. String instability of synchronized flow: (a, b) Simulated vehicle trajectories in synchronized flow in the right lane (a) and left lane (b) at time  $t > T_{ind} + \Delta t$ . (c) Time-functions of speeds of vehicle 1 in the right lane and vehicle 2 in the left lane made by the same numbers in (a, b).

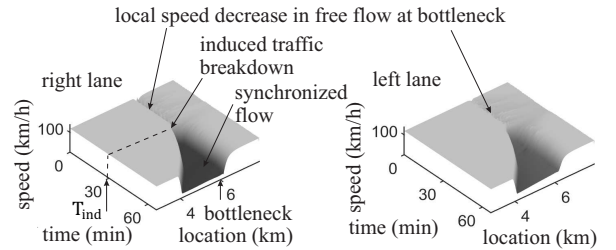


FIG. 37: Nucleation features of  $F \rightarrow S$  transition in automated-driving traffic consisting of 100% TPACC-vehicles (14) under the use of lane-changing and bottleneck models of Sec. II A: Speed in space and time in the right lane (left column) and in left lane (right column).  $\tau_p = 1.3$  s,  $\tau_G = 1.4$  s,  $\tau_{safe} = 1$  s,  $K_1 = 0.3$  s $^{-2}$ ,  $K_{\Delta v} = K_2 = 0.6$  s $^{-1}$ ,  $\tau_1 = \tau_2 = 0.5$  s,  $q_{in} = 2000$  (vehicles/h)/lane,  $q_{on} = 700$  vehicles/h,  $T_{ind} = 30$  min,  $\Delta q_{on} = 200$  vehicles/h,  $\Delta t = 2$  min. Other parameters are the same as those in Fig. 3.

synchronized flow behavior caused by the indifference zone for car-following in the TPACC-model (14). For example, while the velocity of the upstream synchronized flow front for Helly’s model (1), (2) is almost time-independent (Fig. 4), this velocity can depend on time in the TPACC-model (14) (Fig. 37). A more detailed consideration of three-phase traffic theory for automated-driving traffic based on the TPACC-model that could be an interesting subject of scientific investigations is out of scope of this paper.

### C. Conclusions

1. The nucleation nature of traffic breakdown ( $F \rightarrow S$  transition) at a highway bottleneck, which is the basic feature of the three-phase traffic theory for human-driving traffic, has been revealed for vehicular traffic consisting of 100% of automated-driving vehicles moving on a two-lane road with an on-ramp bottleneck. As long as lane changing in free flow ensures a distribution of on-ramp inflow between road lanes, this basic result remains in a broad range of model parameters of automated-driving vehicles.

2. We have found that there is a discontinuity in the rate of lane-changing from the right lane (neighborhood lane to on-ramp) to the left lane (passing lane) (denoted as  $R \rightarrow L$  lane-changing). In its turn, this causes the discontinuity in the over-acceleration rate: The rate of over-acceleration in free flow is larger than it is in synchronized flow.

3. The cause of the nucleation nature of traffic breakdown ( $F \rightarrow S$  transition) in automated-driving vehicular traffic at a bottleneck is the discontinuity in the over-acceleration rate together with the spatiotemporal competition between over-acceleration and speed adaptation. A larger rate of over-acceleration in free flow causes the maintenance of free flow at the bottleneck; contrarily, a lower rate of over-acceleration

in synchronized flow causes the maintenance of synchronized flow at the bottleneck.

4. Through the spatiotemporal competition between over-acceleration and speed adaptation caused by lane-changing, at any time instant there is a range of highway capacities between some minimum and maximum capacities; within the capacity range, an  $F \rightarrow S$  transition can be induced; however, when the maximum capacity is exceeded, then after some time-delay a spontaneous  $F \rightarrow S$  transition occurs at the bottleneck. All three-phases  $F$  (free flow), synchronized flow ( $S$ ), and wide moving jam ( $J$ ) can coexist each other in automated-driving traffic. A diverse variety of phase transitions, which can occur between the phases  $F$ ,  $S$ , and  $J$ , determine the spatiotemporal dynamics of automated-driving vehicular traffic.

5. The discontinuous character of over-acceleration caused by lane-changing is the universal physical feature of vehicular traffic. The three-phase traffic theory is the framework for both human-driving and automated-driving vehicular traffic. Therefore, we can assume that the three-phase traffic theory is also the framework for a mixed traffic consisting of a random distribution of human-driving and automated-driving vehicles. Three-phase traffic theory of mixed traffic that is out of the scope of this paper could be a very interesting task for further traffic studies.

### Acknowledgments

I would like to thank Sergey Klenov for help in simulations and useful suggestions. I thank our partners for their support in the project “LUKAS – Lokales Umfeldmodell für das Kooperative, Automatisierte Fahren in komplexen Verkehrssituationen” funded by the German Federal Ministry for Economic Affairs and Climate Action.

- 
- [1] M.J. Lighthill, G.B. Whitham, Proc. Roy. Soc. A **229**, 281–345 (1955).
  - [2] P.I. Richards, Oper. Res. **4**, 42–51 (1956).
  - [3] A.D. May, *Traffic Flow Fundamentals*, Prentice-Hall, Inc., New Jersey, 1990.
  - [4] C.F. Daganzo, Transp. Res. B **28**, 269–287 (1994); C.F. Daganzo, Transp. Res. B **29**, 79–93 (1995); C.F. Daganzo, *Fundamentals of Transportation and Traffic Operations*, (Elsevier Science Inc., New York, 1997).
  - [5] *Highway Capacity Manual*, Sixth Edition, National Research Council, Transportation Research Board, Washington, DC, 2016.
  - [6] R.P. Roess, E.S. Prassas, *The Highway Capacity Manual: A Conceptual and Research History*, Springer, Berlin, 2014.
  - [7] Daiheng Ni, *Traffic Flow Theory: Characteristics, Experimental Methods, and Numerical Techniques*, (Elsevier, Amsterdam, 2015).
  - [8] R.E. Chandler, R. Herman, E.W. Montroll, Oper. Res. **6** 165–184 (1958).
  - [9] R. Herman, E.W. Montroll, R.B. Potts, R.W. Rothery, Oper. Res. **7** 86–106 (1959).
  - [10] D.C. Gazis, R. Herman, R.B. Potts, Oper. Res. **7** 499–505 (1959).
  - [11] D.C. Gazis, R. Herman, R.W. Rothery, Oper. Res. **9** 545–567 (1961).
  - [12] E. Kometani, T. Sasaki, J. Oper. Res. Soc. Jap. **2**, 11–26 (1958)
  - [13] E. Kometani, T. Sasaki, Oper. Res. **7**, 704–720 (1959)
  - [14] E. Kometani, T. Sasaki, Oper. Res. Soc. Jap. **3**, 176–190 (1961)
  - [15] E. Kometani, T. Sasaki, in *Theory of Traffic Flow*,

- ed. by R. Herman (Elsevier, Amsterdam, 1961), pp. 105–119
- [16] G.F. Newell, *Oper. Res.* **9**, 209–229 (1961); *Transp. Res. B* **36** 195–205 (2002).
- [17] G.F. Newell, “Instability in dense highway traffic, a review”. In: *Proc. Second Internat. Sympos. on Traffic Road Traffic Flow* (OECD, London 1963) pp. 73–83.
- [18] P.G. Gipps, *Trans. Res. B* **15**, 105–111 (1981).
- [19] K. Nagel, M. Schreckenberg, *J. Phys. (France) I* **2** 2221–2229 (1992).
- [20] M. Bando, K. Hasebe, A. Nakayama, A. Shibata, and Y. Sugiyama, *Jpn. J. Appl. Math.* **11**, 203 (1994); *Phys. Rev. E* **51**, 1035 (1995).
- [21] D. Chowdhury, L. Santen, A. Schadschneider, *Phys. Rep.* **329** 199–329 (2000).
- [22] D. Helbing, *Rev. Mod. Phys.* **73** 1067–1141 (2001).
- [23] T. Nagatani, *Rep. Prog. Phys.* **65** 1331–1386 (2002).
- [24] K. Nagel, P. Wagner, R. Woessler, *Oper. Res.* **51** 681–716 (2003).
- [25] M. Saifuzzaman, Z. Zheng, *Transp. Res. C* **48** 379–403 (2014).
- [26] A. Schadschneider, D. Chowdhury, K. Nishinari, *Stochastic Transport in Complex Systems* (Elsevier Science Inc., New York, 2011).
- [27] M. Treiber, A. Kesting, *Traffic Flow Dynamics*, (Springer, Berlin, 2013)
- [28] W.D. Ashton, *The theory of traffic flow*, (Methuen & Co. London, John Wiley & Sons, New York, 1966).
- [29] D.L. Gerlough, M.J. Huber, *Traffic Flow Theory Special Report 165*, (Transp. Res. Board, Washington D.C., 1975).
- [30] D.C. Gazis, *Traffic Theory*, (Springer, Berlin, 2002).
- [31] J. Barceló (ed.), *Fundamentals of Traffic Simulation*, (Springer, Berlin, 2010).
- [32] L. Elefteriadou, *An Introduction to Traffic Flow Theory*, (Springer, Berlin, 2014).
- [33] F. Kessels, *Traffic flow modelling*, (Springer, Berlin, 2019).
- [34] B.S. Kerner, P. Konhäuser, *Phys. Rev. E* **48**, R2335 (1993); *Phys. Rev. E* **50**, 54–83 (1994)
- [35] P.A. Ioannou, E.B. Kosmatopoulos, *Adaptive Control*, in: John G. Webster (Ed.), *Wiley Encyclopedia of Electrical and Electronics Engineering*, John Wiley & Sons, Inc., New York, 2000, <https://doi.org/10.1002/047134608X.W1002>.
- [36] P.A. Ioannou, C.C. Chien, *IEEE Trans. Veh. Tech.* **42** (1993) 657–672.
- [37] W. Levine, M. Athans, *IEEE Trans. Automat. Contr.* **11** (1966) 355–361.
- [38] C-Y Liang, H. Peng, *Veh. Syst. Dyn.* **32** (1999) 313–330.
- [39] C-Y Liang, H. Peng, *JSME Jnt. J. Ser. C* **43** (2000) 671–677.
- [40] D. Swaroop, J.K. Hedrick, *IEEE Trans. Automat. Contr.* **41** (1996) 349–357; D. Swaroop, J.K. Hedrick, S.B. Choi, *IEEE Trans. Veh. Technol.* **50** (2001) 150–161.
- [41] P. Varaiya, *IEEE Trans. Aut. Cont.* **38** (1993) 195–207.
- [42] T.-W. Lin, S.-L. Hwang, P. Green, *Safety Science* **47** (2009) 620–625.
- [43] J.-J. Martinez, C. Canudas-do-Wit, *IEEE Trans. Cont. Syst. Tech.* **15** (2007) 246–258.
- [44] J. Van Brummelen, M. O’Brien, D. Gruyer, H. Najjaran, *Transp. Res. C* **89** (2018) 384–406.
- [45] S.E. Shladover, *Veh. Syst. Dyn.* **24** (1995) 551–595; S.E. Shladover, D. Su, X.-T. Lu, *Transp. Res. Rec.* **2324** (2012) 63–70.
- [46] R. Rajamani, *Vehicle Dynamics and Control*, Mechanical Engineering Series. Springer US, Boston, 2012.
- [47] L.C. Davis, *Phys. Rev. E* **69** (2004) 066110.
- [48] L.C. Davis, *Physica A* **405** (2014) 128–139.
- [49] L.C. Davis, *Physica A* **451** (2016) 320–332; L.C. Davis, *Physica A* **368** (2006) 541–550; L.C. Davis, *Physica A* **361** (2006) 606–618; L.C. Davis, *Physica A* **379** (2007) 274–290; L.C. Davis, *Physica A* **387** (2008) 6395–6410.
- [50] R. Schmitz, M. Torrent-Moreno, H. Hartenstein, W. Effelsberg, in *29th Annual IEEE International Conference on Local Computer Networks*, 2004, pp. 594–601.
- [51] J. Maurer, T. Fuegen, W. Wiesbeck, in *11th European Wireless Conference 2005 – Next Generation wireless and Mobile Communications and Services*, 2006, pp. 1–7.
- [52] Q. Chen, D. Jiang, V. Taliwal, L. Delgrossi, in *Proceedings of the 3rd international workshop on Vehicular ad hoc networks (VANET ’06)*, (Association for Computing Machinery, New York, NY, 2006), pp. 50–56.
- [53] T.-H. Wang, S. Manivasagam, M. Liang, B. Yang, W. Zeng, R. Urtasun, in *Computer Vision – ECCV 2020. ECCV 2020. Lecture Notes in Computer Science, vol. 12347*, ed. by A. Vedaldi, H. Bischof, T. Brox, JM. Frahm. (Springer, Cham., 2020). [https://doi.org/10.1007/978-3-030-58536-5\\_36](https://doi.org/10.1007/978-3-030-58536-5_36)
- [54] W. Chen (Ed.). *Vehicular Communications and Networks* (Woodhead Publishings, Cambridge, 2015).
- [55] S. Dharba, K.R. Rajagopal, *Transp. Res. C* **7** (1999) 329–352.
- [56] G. Marsden, M. McDonald, M. Brackstone, *Transp. Res. C* **9** (2001) 33–51.
- [57] H. Krishnan, *Transp. Res. Rec.* **1748** (2001) 167–174.
- [58] J. VanderWerf, S.E. Shladover, M. Miller, N. Kourjanskaia, *Transp. Res. Rec.* **1800** (2002) 78–84.
- [59] P.Y. Li, A. Shrivastava, *Transp. Res. C* **10** (2002) 275–301.
- [60] S. Kukuchi, N. Uno, M. Tanaka, *Transp. Eng.* **129** (2003) 146–154.
- [61] A. Bose, P. Ioannou, *Transp. Res. C* **11** (2003) 439–462.
- [62] H. Suzuki, *JSAE Rev.* **24** (2003) 403–410.
- [63] J. Zhou, H. Peng, *IEEE Trans. Intell. Transp. Syst.* **6** (2005) 229–237.
- [64] B. van Arem, C.J.G. van Driel, R. Visser, *IEEE Trans. on ITS* **7** (2006) 429–436.
- [65] M. Treiber, D. Helbing, *Automatisierungstechnik* **49** (2001) 478–484; A. Kesting, M. Treiber, M. Schönhof, D. Helbing, *Transp. Res. Rec.* **2000** (2007) 16–24; A. Kesting, M. Treiber, M. Schönhof, D. Helbing, *Transp. Res. C* **16** (2008) 668–683; A. Kesting, M. Treiber, D. Helbing, *Phil. Trans. Royal Soc. A* **368** (2010) 4585–4605.
- [66] D. Ngoduy, *Transpormetrica* **8** (2012) 43–60; D. Ngoduy, *Comm. Non. Sci. & Numer. Sim.* **18** (2013) 2838–2851.
- [67] A.I. Delis, I.K. Nikolos, M. Papageorgiou, *Comp. & Math. Appl.* **70** (2015) 1921–1947; I.A. Ntousakis, I.K. Nikolos, M. Papageorgiou, *Transp. Res. Procedia* **9** (2015) 111–127; C. Roncoli, M. Papageorgiou, I. Papamichail, *Transp. Res. C* **57** (2015) 241–259; G.

- Perraki, C. Roncoli, I. Papamichail, M. Papageorgiou, *Trans. Res. C* 92 (2018) 456–471.
- [68] A. Talebpour, H.S. Mahmassani, *Transp. Res. C* 71 (2016) 143–163.
- [69] R. Wang, Y. Li, D.B. Work, *Transp. Res. C* 78 (2017) 95–110.
- [70] M. Mamouei, I. Kaparias, G. Halikias, *Transp. Res. C* 92 (2018) 27–41.
- [71] G. Sharon, M.W. Levin, J.P. Hanna, T. Rambha, S.D. Boyles, P. Stone, *Transp. Res. C* 84 (2017) 142–157.
- [72] Y. Han, S. Ahn, *Transp. Res. B* 107 (2018) 146–166; D. Chen, S. Ahn, M. Chitturi, D.A. Noyce, *Transp. Res. B* 100 (2017) 196–221.
- [73] M. Zhou, X. Qu, S. Jin, *IEEE Trans. ITS* 18 (2017) 1422–1428.
- [74] M. Klawtanong, S. Limkumnerd, *Physica A* 542 (2020) 123412.
- [75] G. Zhang, Y. Zhang, D.-B. Pan, R.-J. Huang, *Physica A* 534 (2019) 122029.
- [76] H.B. Zhu, Y.J. Zhou, W.J. Wu, *Physica A* (2020), DOI: 10.1016/j.physa.2020.124337.
- [77] J. Zhou, F. Zhu, *Trans. Res. C* 115 (2020) 102614.
- [78] Y. Zhou, S. Ahn, M. Wang, S. Hoogendoorn, *Transp. Res. B* 132 (2020) 152–170.
- [79] D. Chen, A. Srivastava, S. Ahn, T. Li, *Transp. Res. C* 113 (2020) 260–276.
- [80] Z. Zhong, E. E. Lee, M. Nejad, J. Lee, *Transp. Res. C* 115 (2020) 102611.
- [81] F.-f. Zheng, C. Liu, X. Liu, S. E. Jabari, L. Lu, *Transp. Res. C* 112 (2020) 203–219.
- [82] S. Jin, D.-H. Sun, M. Zhao, Y. Li, J. Chen, *Physica A* 551 (2020) 124217.
- [83] Y.J. Zhou, H.B. Zhu, M.M. Guo, J.L. Zhou, *Physica A* 540 (2020) 122721.
- [84] Z. Yao, R. Hu, Y. Wang, Y. Jiang, B. Ran, Y. Chen, *Physica A* 533 (2019) 121931.
- [85] L. Ye, T. Yamamoto, *Physica A* 526 (2019) 121009.
- [86] W.-X. Zhu, H. M. Zhang, *Physica A* 496 (2018) 274–285.
- [87] Z. Wen-Xing, Z. Li-Dong, *Physica A* 492 (2018) 2154–2165.
- [88] A L. Ye, T. Yamamoto, *Physica A* 490 (2018) 269–277; L. Ye, T. Yamamoto, *Physica A* 512 (2018) 588–597.
- [89] Xin Chang, Haijian Li, Jian Rong, Xiaohua Zhao, An'ran Li, *Physica A* 557 (2020) 124829.
- [90] B.S. Kerner, *Trans. Res. Rec.* **1678**, 160–167 (1999); in *Transportation and Traffic Theory*, ed. by A. Ceder. (Elsevier Science, Amsterdam 1999), pp. 147–171; *Physics World* **12**, 25–30 (August 1999); *Trans. Res. Rec.* **1710**, 136–144 (2000); *Net. Spat. Economics* **1** 35–76 (2001); *Phys. Rev. E* **65** 046138 (2002); *Trans. Res. Rec.* **1802**, 145–154 (2002); *Math. Comp. Modelling* **35** 481–508 (2002).
- [91] B.S. Kerner, *J. Phys. A: Math. Gen.* **33** L221–L228 (2000); in: D. Helbing, H.J. Herrmann, M. Schreckenberg, D.E. Wolf (Eds.), *Traffic and Granular Flow'99: Social, Traffic and Granular Dynamics*, Springer, Heidelberg, Berlin, 2000, pp. 253–284.
- [92] B.S. Kerner, *Phys. Rev. Lett.* **81**, 3797–3400 (1998); in: *Proc. of the Third Int. Sym. on Highway Capacity* (Rikke Rysgaard, ed.) Road Directorate, Ministry of Transport – Denmark, pp. 621–641 (1998).
- [93] B.S. Kerner, *The Physics of Traffic* (Springer, Berlin, New York 2004)
- [94] B.S. Kerner, *Introduction to Modern Traffic Flow Theory and Control*. (Springer, Berlin, New York, 2009).
- [95] B.S. Kerner, *Breakdown in Traffic Networks*. (Springer, Berlin, New York, 2017).
- [96] B.S. Kerner, *Understanding Real Traffic*. (Springer, Cham, Switzerland, 2021).
- [97] B.S. Kerner, in: B.S. Kerner (Ed.), *Complex Dynamics of Traffic Management*, Encyclopedia of Complexity and Systems Science Series, Springer, New York, NY, 2019, pp. 21–77.
- [98] B.S. Kerner, M. Koller, S.L. Klenov, H. Rehborn, M. Leibel, *Physica A* **438**, 365–397 (2015).
- [99] B. S. Kerner, H. Rehborn, R.-P. Schäfer, S. L. Klenov, J. Palmer, S. Lorkowski, and N. Witte, *Physica A* **392**, 221 (2013).
- [100] B.S. Kerner, S.L. Klenov, *J. Phys. A: Math. Gen.* **35**, L31–L43 (2002).
- [101] B.S. Kerner, S.L. Klenov, D.E. Wolf, *J. Phys. A: Math. Gen.* **35**, 9971–10013 (2002)
- [102] B.S. Kerner, S.L. Klenov, *Phys. Rev. E* **68** 036130 (2003); B.S. Kerner, S.L. Klenov, *J. Phys. A: Math. Gen.* **37**, 8753–8788 (2004); B.S. Kerner, S.L. Klenov, *J. Phys. A: Math. Gen.* **39**, 1775–1809 (2006); B.S. Kerner, S.L. Klenov, A. Hiller, *J. Phys. A: Math. Gen.* **39**, 2001–2020 (2006); B.S. Kerner, S.L. Klenov, *Phys. Rev. E* **80** 056101 (2009); B.S. Kerner, *J. Phys. A: Math. Theor.* **41** 215101 (2008); B. S. Kerner, *Phys. Rev. E*, **85**, 036110 (2012); B.S. Kerner, in *Complex Dynamics of Traffic Management*, ed. by B.S. Kerner, Encyclopedia of Complexity and Systems Science Series (Springer, New York, NY, 2019), pp. 389–500
- [103] L.C. Davis, *Phys. Rev. E* **69** 016108 (2004); L.C. Davis, *Physica A* **388** 4459–4474 (2009); L.C. Davis, *Physica A* **389** 3588–3599 (2010); L.C. Davis, *Physica A* **391** 1679 (2012).
- [104] H.K. Lee, R. Barlović, M. Schreckenberg, D. Kim, *Phys. Rev. Lett.* **92** 238702 (2004); A. Pottmeier, C. Thiemann, A. Schadschneider, M. Schreckenberg, in: A. Schadschneider, T. Pöschel, R. Kühne, M. Schreckenberg, D.E. Wolf (Eds.), *Traffic and Granular Flow'05*, Springer, Berlin, 2007, pp. 503–508; H.-K. Lee, B.-J. Kim, *Physica A* **390** 4555–4561 (2011).
- [105] R. Jiang, Q.-S. Wu, *J. Phys. A: Math. Gen.* **37** 8197–8213 (2004); K. Gao, R. Jiang, S.-X. Hu, B.-H. Wang, Q.-S. Wu, *Phys. Rev. E* **76** 026105 (2007).
- [106] X.G. Li, Z.Y. Gao, K.P. Li, X.M. Zhao, *Phys. Rev. E* **76** 016110 (2007).
- [107] K. Hausken, H. Rehborn, *Game Theoretic Analysis of Congestion, Safety and Security*, in: Springer Series in Reliability Engineering, Springer, Berlin, 2015, pp. 113–141.
- [108] J-f Tian, C. Zhu, R Jiang, in: B.S. Kerner (Ed.) *Complex Dynamics of Traffic Management*, A Volume in the Encyclopedia of Complexity and Systems Science, Second Edition (Springer, New York, NY, 2019), pp. 313–342
- [109] J.-W. Zeng, Y.-S. Qian, Z. Lv, F. Yin, L. Zhu, Y. Zhang, D. Xu, *Physica A* **574**, 125918 (2021); J.-W. Zeng, Y.-S. Qian, S.-B. Yu, X.-T. Wei, *Physica A* **530**, 121567 (2019)
- [110] H.-T. Zhao, L. Lin, C.-P. Xu, Z.-X. Li, X. Zhao, *Physica A* **553**, 124213 (2020)
- [111] J.J. Wu, H.J. Sun, Z.Y. Gao, *Phys. Rev. E* **78**, 036103 (2008)
- [112] H. Yang, J. Lu, X.-J. Hu, J. Jiang, *Physica A* **392**,



- 4009–4018 (2013)
- [113] H. Yang, X. Zhai, C. Zheng, *Physica A* **509**, 567–577 (2018)
- [114] F. Siebel, W. Mauser, *Phys. Rev. E* **73**, 066108 (2006)
- [115] F. Rempe, P. Franek, U. Fastenrath, K. Bogenberger, *Transp. Res. C* **85**, 644–663 (2017)
- [116] H. Rehborn, S.L. Klenov, in *Encyclopedia of Complexity and System Science*, ed. by R.A. Meyers (Springer, Berlin, 2009), pp. 9500–9536; H. Rehborn, S.L. Klenov, M. Koller, in *Complex Dynamics of Traffic Management*, ed. by B.S. Kerner, Encyclopedia of Complexity and Systems Science Series (Springer, New York, NY, 2019), pp. 501–557
- [117] H. Rehborn, S.L. Klenov, J. Palmer, *Physica A* **390**, 4466–4485 (2011); H. Rehborn, J. Palmer, *Intell. Veh. Sym. IEEE*, 2008, pp. 186–191; H. Rehborn, S.L. Klenov, J. Palmer, *IEEE Intell. Veh. Sym. (IV)*, 2011, pp 19–24; H. Rehborn, M. Koller, *J. of Adv. Transp.* **48**, 1107–1120 (2014).
- [118] H. Rehborn, M. Koller, S. Kaufmann, *Data-Driven Traffic Engineering: Understanding of Traffic and Applications based on Three-Phase Traffic Theory*, (Elsevier, Amsterdam, 2021)
- [119] Y.-S. Qian, X. Feng, J.-W. Zeng, *Physica A* **479**, 509–526 (2017)
- [120] J.P.L. Neto, M.L. Lyra, C.R. da Silva, *Physica A* **390**, 3558–3565 (2011)
- [121] X.-j. Hu, H. Liu, X. Hao, Z. Su Z. Yang, *Physica A* **563**, 125495 (2021); X.-j. Hu, F. Zhang, J. Lu, M.-y. Liu, Y.-f. Ma, Q. Wan, *Physica A* **527**, 121176 (2019); X.-j. Hu, X.-t. Hao, H. Wang, Z. Su, F. Zhang, *Physica A* **545**, 123725 (2020); X.-j. Hu, L.-q. Qiao, X.-t. Hao, C.-x. Lin, T.-h. Liu, *Physica A*, **605** 127962 (2022).
- [122] D.-J. Fu, Q.-L. Li, R. Jiang, B.-H. Wang, *Physica A* **559** 125075 (2020); Q.-L. Li, J.-X. Wang, L.-L. Ye, R. Jiang and B.-H. Wang, *Int. J. Mod. Phys. C* (2023), DOI: 10.1142/S0129183123501206.
- [123] R. Borsche, M. Kimathi, A. Klar, *Comput. Math. Appl.* **64**, 2939–2953 (2012).
- [124] V. Wiering, S.L. Klenov, B.S. Kerner, M. Schreckenberg, *Phys. Rev. E* **106**, 054306 (2022).
- [125] B.S. Kerner, *Phys. Rev. E* **97** 042303 (2018); B.S. Kerner, *Physica A* **562**, 125315 (2021); B.S. Kerner, *Procedia Computer Science* **130** 785–790 (2018), B.S. Kerner, in: B.S. Kerner (Ed.), *Complex Dynamics of Traffic Management*, Encyclopedia of Complexity and Systems Science Series, Springer, New York, NY, 2019, pp. 343–385.
- [126] W. Helly, in: *Proceedings of the Symposium on Theory of Traffic Flow*, pp. 207–238, Research Laboratories, General Motors, Elsevier, Amsterdam (1959).
- [127] K. Nagel, D. E. Wolf, P. Wagner, and P. Simon, *Phys. Rev. E* **58**, 1425 (1998).
- [128] B. S. Kerner and S. L. Klenov, *J. Phys. A: Math. Theor.* **43**, 425101 (2010).
- [129] B.S. Kerner, German patent publications DE 000010308256a1, 2004; DE 102007008253a1, 2007; DE 102007008257a1, 2007; DE 102007008254a1, 2008; USA patents US 20070150167A1, 2007; US 7451039B2, 2008.
- [130] In more details, this criticism of standard traffic models can be found in books [93–96]; in particular, see Appendix C in [96].
- [131] See explanations of the term *over-acceleration* in Sec. 8.1.5 of the book [96].
- [132] In [90, 91, 93], the probability of over-acceleration shown in Fig. 2 (a) has been called “probability of passing” (see Fig. 5.7 (b) of the book [93]).
- [133] These equations are solved with the second-order Runge-Kutta method with time step  $10^{-2}$ . No noticeable changes in simulation results have been found when time step of calculation has been reduced to  $10^{-3}$  s.
- [134] The exclusion is a discussion in Sec. VIA, in which we compare traffic phenomena at the bottleneck under string-stability condition (3) studied in Secs. II–V with traffic phenomena occurring in free flow at the same bottleneck, when automated vehicles do not satisfy condition for string stability (3).
- [135]  $R_{RL}$  is the number of automated vehicles that change from the right lane to the left lane during a time unit within the road region  $x_{on} - L_{RL} \leq x \leq x_{on} + L_m$ , where parameter  $L_{RL} = 0.06\text{--}0.1$  km used in simulations should guarantee that R→L lane-changing at the upstream front of synchronized flow (after the F→S transition has occurred, see Sec. IIE) does not come in the calculation of  $R_{RL}$ .
- [136] The mean time headway between vehicles in free flow is equal to  $\tau_{\text{mean}}^{(\text{free})} = (3600/q_{in}) - (d/v_{\text{free}}) \approx 1.175$  s.
- [137] It should be emphasized that the free flow state at the bottleneck shown in Fig. 4 during time interval  $0 \leq t < T_{\text{ind}}$  is *identical* with the free flow state at the bottleneck in Fig. 3. Therefore, parameters of trajectories shown in Fig. 5 are related to both Fig. 3 and to Fig. 4 for time interval  $0 \leq t < T_{\text{ind}}$ .
- [138] This MB model is the same as that in [128] used in a stochastic discrete microscopic model for human-driving traffic.
- [139] It must be emphasized that we study a *deterministic* model of automated-driving vehicular traffic of Sec. IIA, in which *no random* local disturbances of speed, flow rate, or/and density occur. Rather than through random effects, in such a “deterministic limit” of the three-phase traffic theory, local disturbances appear *only* through vehicle interactions with each other. In particular, such vehicle interactions are caused by vehicle merging at the on-ramp bottleneck as well as by lane-changing behavior. For this reason, if  $q_{\text{sum}} = C_{\text{max}}$ , then the traffic system is in a “intermediate” free flow state in which any (even very small) addition time-limited local speed decrease at the bottleneck causes an F→S transition at the bottleneck. It has been proven that the smaller the time-limited additional local speed decrease at the bottleneck is, the longer the time delay  $T^{(B)}$  of the F→S transition at the bottleneck.
- [140] The rate  $R_{OA}$  in free flow is nearly the same as that when condition (12) is not used (Secs. II–IV B).
- [141] Note that for Helly’s model (1), (2) with  $\tau_d = 1.5$  s, we have found  $q_{\text{on,max}}^{(1\text{-lane})} - q_{\text{on,min}} = 10$  vehicles/h.